



This is a repository copy of *Quantifying mechanisms of aeolian dust emission : field measurements at Etosha Pan, Namibia.*

White Rose Research Online URL for this paper:

<https://eprints.whiterose.ac.uk/190241/>

Version: Published Version

Article:

Wiggs, G.F.S., Baddock, M.C., Thomas, D.S.G. et al. (7 more authors) (2022) Quantifying mechanisms of aeolian dust emission : field measurements at Etosha Pan, Namibia. *Journal of Geophysical Research: Earth Surface*, 127 (8). ISSN 2169-9003

<https://doi.org/10.1029/2022jf006675>

Reuse

This article is distributed under the terms of the Creative Commons Attribution (CC BY) licence. This licence allows you to distribute, remix, tweak, and build upon the work, even commercially, as long as you credit the authors for the original work. More information and the full terms of the licence here:

<https://creativecommons.org/licenses/>

Takedown

If you consider content in White Rose Research Online to be in breach of UK law, please notify us by emailing eprints@whiterose.ac.uk including the URL of the record and the reason for the withdrawal request.



eprints@whiterose.ac.uk
<https://eprints.whiterose.ac.uk/>



Quantifying Mechanisms of Aeolian Dust Emission: Field Measurements at Etosha Pan, Namibia

Key Points:

- Ground-based data show aeolian dust emissions occur throughout the year, not restricted to winter as indicated by satellite observations
- Emissions are largely driven by low-level jets in the dry winter, and by cold pool outflows in the more humid summer
- The magnitude of emissions is dominated by only a few events, with six events accounting for nearly 31% of all horizontal dust flux

Supporting Information:

Supporting Information may be found in the online version of this article.

Correspondence to:

G. F. S. Wiggs,
giles.wiggs@ouce.ox.ac.uk

Citation:

Wiggs, G. F. S., Baddock, M. C., Thomas, D. S. G., Washington, R., Nield, J. M., Engelstaedter, S., et al. (2022). Quantifying mechanisms of aeolian dust emission: Field measurements at Etosha Pan, Namibia. *Journal of Geophysical Research: Earth Surface*, 127, e2022JF006675. <https://doi.org/10.1029/2022JF006675>

Received 15 MAR 2022

Accepted 27 JUL 2022

Author Contributions:

Conceptualization: Giles F. S. Wiggs, David S. G. Thomas, Richard Washington
Formal analysis: Giles F. S. Wiggs, Matthew C. Baddock, Joanna M. Nield, Sebastian Engelstaedter, Robert G. Bryant
Funding acquisition: Giles F. S. Wiggs, David S. G. Thomas, Richard Washington
Investigation: Giles F. S. Wiggs, Matthew C. Baddock, David S. G. Thomas, Richard Washington, Joanna M. Nield, Sebastian Engelstaedter, Robert G. Bryant, Frank D. Eckardt, Johannah R. C. von Holdt, Shayne Kötting

Giles F. S. Wiggs¹, Matthew C. Baddock², David S. G. Thomas¹, Richard Washington¹, Joanna M. Nield³, Sebastian Engelstaedter¹, Robert G. Bryant⁴, Frank D. Eckardt⁵, Johannah R. C. von Holdt⁵, and Shayne Kötting⁶

¹School of Geography and the Environment, University of Oxford, Oxford, UK, ²Geography and Environment, Loughborough University, Loughborough, UK, ³School of Geography and Environmental Science, University of Southampton, Southampton, UK, ⁴Department of Geography, University of Sheffield, Sheffield, UK, ⁵Department of Environmental and Geographical Science, University of Cape Town, Cape Town, South Africa, ⁶Ministry of Environment, Forestry and Tourism, Etosha National Park, Windhoek, Namibia

Abstract Determining the controls on aeolian dust emissions from major sources is necessary for reliable quantification of atmospheric aerosol concentrations and fluxes. However, ground-based measurements of dust emissions at-source are rare and of generally short duration, failing to capture the annual cycle. Here, we provide new insights into dust dynamics by measuring aerosol concentrations and meteorological conditions for a full year (July 2015–June 2016) at Etosha Pan, Namibia, a globally significant dust source. Surface deployed field instrumentation provided 10-min averaged data on meteorological conditions, aerosol concentration (mg/m^3), and horizontal dust flux ($\text{g}/\text{m}^2/\text{min}_{10}$). A Doppler lidar provided additional data for some of the period. 51 significant dust events were identified in response to strong E-ENE winds. We demonstrate that these events occurred throughout the year and were not restricted to the austral winter, as previously indicated by satellite observations. Peak horizontal flux occurred in the spring (November) due to strengthening erosive winds and highly desiccating conditions increasing surface erodibility. We identify a strong seasonal differentiation in the meteorological mechanisms controlling dust uplift; low-level jets on dry winter mornings (61% of all events), and cold pool outflows in humid summer evenings (39% of events). Significantly, we demonstrate a very strong bias toward the contribution of low frequency and high magnitude events, with nearly 31% of annual horizontal dust flux generated by only 6 individual events. Our study demonstrates how longer-term (≈ 1 year), ground-based, and at-source field measurements can radically improve interpretations of dust event dynamics and controls at major source locations.

Plain Language Summary Atmospheric dust is important because it affects climate, human health, and nutrient distribution. Most atmospheric dust is sourced from dry lake beds in deserts and much of our understanding of dust emission comes from satellite observations. Few field studies have measured dust emission from such sources for more than a few months and so our understanding of the processes that govern dust emission is partial. We measured dust concentrations and associated meteorological conditions for a full year at Etosha Pan in Namibia, a major source of dust globally. We found that dust emission occurred throughout the year, not just in winter as had previously been thought. Our data showed that the meteorological mechanisms controlling dust emission changed seasonally. In dry winter mornings dust was eroded by jets of fast-moving winds soon after sunrise. In summer, emission occurred in the late evenings due to high-speed winds associated with the development of convective storms. Further, dust emission was dominated by high magnitude and low frequency events. Our field data demonstrate the seasonal complexity in the controlling mechanisms of dust emission which need to be accounted for in calculations of atmospheric dust loading.

1. Introduction

Windblown dust is a major global export from the world's deserts and plays a critical role in the Earth's land-atmosphere-ocean-biosphere system (Shao et al., 2011). It has been shown to have a crucial influence on the radiation balance and climate modulation (Evan et al., 2016; Kok et al., 2017; Li et al., 2004; Schepanski, 2018; Slingo et al., 2006; Zhu et al., 2007), iron fertilization of the ocean (Cassar et al., 2007; Dansie et al., 2018, 2022; Ito & Kok, 2017; Jickells et al., 2005), long-distance nutrient transport and soil geochemistry (Bristow et al., 2010; Koren et al., 2006; Lawrence et al., 2013), and human health (O'Hara et al., 2000; Prospero et al., 2014; Stafoggia

© 2022. The Authors.

This is an open access article under the terms of the [Creative Commons Attribution License](https://creativecommons.org/licenses/by/4.0/), which permits use, distribution and reproduction in any medium, provided the original work is properly cited.

Methodology: Giles F. S. Wiggs, David S. G. Thomas, Richard Washington, Robert G. Bryant, Shayne Kötting

Project Administration: Giles F. S. Wiggs

Writing – original draft: Giles F. S. Wiggs, Matthew C. Baddock, David S. G. Thomas, Richard Washington, Joanna M. Nield, Sebastian Engelstaedter, Robert G. Bryant, Frank D. Eckardt, Johannah R. C. von Holdt

Writing – review & editing: Giles F. S. Wiggs, Matthew C. Baddock, David S. G. Thomas, Joanna M. Nield, Sebastian Engelstaedter, Robert G. Bryant, Frank D. Eckardt, Johannah R. C. von Holdt

et al., 2016). Yet the complex controls governing the emission of dust and the dynamics of individual dust emission events, which together represent the activity of emissive source areas, remain poorly understood (Bryant, 2013; Bullard, 2010). Such uncertainties in characterizing source behavior lead to significant challenges for the development of models representing dust emission into the atmosphere (Darmenova et al., 2009; Haustein et al., 2015; Klose et al., 2019; Kok, Albani, et al., 2014; Kok, Mahowald, et al., 2014; Zhao et al., 2022) and, in turn, for effectively modeling the effect of mineral dust on climate (Sokolik & Toon, 1999).

Dust emission characteristics and fluxes from major desert sources have not been quantified effectively, and one of the reasons for this is a scarcity of ground-based, at-source measurements of aerosol concentrations, or well-resolved information on dust event dynamics (Bryant, 2013; Bullard, 2010; Haustein et al., 2015; Klose et al., 2019). A key problem is related to the difficulty in collecting relevant ground-based data from highly emissive source areas that predominantly consist of discrete, large-scale, endorheic, dry lake beds in relatively inaccessible desert locations (Mahowald et al., 2003; Prospero et al., 2002; Washington et al., 2003). Our recent knowledge of dust emission dynamics has therefore been derived primarily from satellite remote sensing studies which, whilst successfully offering data on emission source locations (e.g., Ashpole & Washington, 2013; Baddock et al., 2016; Caton Harrison et al., 2019; Ginoux et al., 2012; Murray et al., 2016; Schepanski et al., 2009; von Holdt et al., 2017) and event frequencies (e.g., Bryant et al., 2007; Vickery et al., 2013), do not alone provide the high temporal and spatial resolution measurements required to robustly identify dust emission drivers and event characteristics, nor provide the most appropriate data for adequate quantification of event magnitudes (e.g., Baddock et al., 2021; Bryant & Baddock, 2021).

Ground-based observations of aeolian dust fluxes and boundary-layer climatology have the potential to fill this fundamental data gap, but appropriate field monitoring campaigns at highly emissive source areas are uncommon (Bryant, 2013). There are several field studies that have measured meteorological and dust flux characteristics for large, individual dust events (e.g., Zobeck & Van Pelt, 2006), but these are often several hundred kilometres downwind from the emissive source and so provide limited data on emissions controls (e.g., Baddock et al., 2015; Leys et al., 2011; McTainsh et al., 2005). There are also examples of larger-scale field campaigns focused on measurements of meteorology and aerosols arising from several sources at the regional scale. These include the FENNEC campaign in the central Sahara (e.g., Allen et al., 2015; Allen & Washington, 2014; Marsham et al., 2013; Todd et al., 2013), and the AMMA campaign focused on mineral dust and biomass burning in the Sahel region of Africa (e.g., Kaly et al., 2015; Marticorena et al., 2010, 2017; Rajot et al., 2008; Sow et al., 2009).

Examples of field campaigns coupling boundary-layer climatology and dust emissions at and from specific emissions sources are notably lacking, but have provided considerable benefits. A classic and intensive study was focused on Owens Lake (USA) in the 1990s. This offered comprehensive field data of great value in terms of understanding dust drivers, but only for a small emissions source (e.g., Cahill et al., 1996; Gillette et al., 1997; Niemeyer et al., 1999; Reid et al., 1994). Elsewhere, informative field datasets have been obtained from a short-term and spatially-discrete study in the Bodélé depression (Todd et al., 2007; Washington et al., 2006), while some high spatial resolution field data are available from the DO4Models project in Sua Pan, Botswana (Haustein et al., 2015). These field campaigns in the Bodélé and Sua evidenced how valuable even short-term “at-source” surface observations can be in constraining and evaluating the performance of numerical dust emission schemes. Additional ground-based monitoring of dust emissions from specific sources has been carried out in the ephemeral river valleys of Namibia (Dansie et al., 2017; von Holdt et al., 2019) and, more recently, on the western edge of Etosha Pan, also in Namibia (Clements & Washington, 2021). Typically, field campaigns focus on specific properties of the emissions process and, for ease of measurement and given the complexity of system heterogeneity, consider only small and spatially discrete dust emissions sources (e.g., Khalfallah et al., 2020; Webb et al., 2021) over relatively short durations, spanning only a season of dust emissions of $\approx 2\text{--}3$ months (e.g., Shao et al., 2020). Such research approaches take no account of the annual cycle of emissions in environments where climatic seasonality is a dominant feature.

Realistic modeling of the dust cycle begins with the proper inclusion of emission activity in source areas (e.g., Haustein et al., 2015). Such ambition cannot be achieved without ground-based measurements of the drivers and fluxes of dust emission events and a detailed understanding of the atmospheric and land surface dynamics that control dust uplift. Such ground-based data over an annual cycle are vital and can add considerable value to the more pervasive aerosol information available from the remote sensing record. Here, we begin to address the deficiency of at-source dust observations by undertaking field measurements of dust event dynamics and

surface boundary layer characteristics at Etosha Pan in Namibia, a globally significant dust source (Washington et al., 2003). We use a suite of comprehensive ground-based measurements, and a measurement framework developed during prior dust emissions research at Sua Pan (Haustein et al., 2015), to uniquely characterize drivers of dust activity at both seasonal and event scales over a period of 12 months. Our objective is to identify seasonally changing mechanisms that drive dust emission and demonstrate the variable contribution of individual emissions events to overall dust flux. In this way we aim to provide the first quantification of magnitude-frequency relationships for dust emissions over a sustained monitoring period at a globally significant dust source.

2. Etosha Pan, Namibia

Etosha Pan in semi-arid northern Namibia (18.80°S, 16.30°E; Figure 1) consists of a 5,000–6,000 km² hydrologically-ephemeral basin rich in fine clay and silt sediments (Bhattachan et al., 2015; Hipondoka et al., 2014). The pan lies at 1,080 m asl (Bryant, 2003) and is an endorheic basin at the terminus of a drainage system covering northern Namibia and southern Angola (Buch & Rose, 1996). Mean annual rainfall in the region varies from 400 to 450 mm with the vast majority falling in the summer months generally from October–April (Bryant, 2003). Rain periodically drives the ephemeral drainage system to the north of Etosha, which is thought to supply fine-grained fluvial sediment to the pan during periods of partial and occasional inundation (Bryant, 2003; Mahowald et al., 2003). In the dry winter months (July–September) the below-pan water table lowers and the surface of the pan can become susceptible to deflation by the erosive E-NE winds, resulting in significant dust emission events (Vickery et al., 2013; Figure 1).

Investigations of dust events over Etosha Pan using a variety of remote sensing products (e.g., TOMS AI, MODIS, SEVIRI, AVHRR) highlight the pan as being one of the most significant windblown dust sources in the southern hemisphere and one of the top 10 most significant sources globally (Bryant, 2003; Bryant et al., 2007; Ginoux et al., 2012; Vickery et al., 2013; Washington et al., 2003). From analysis of remote sensing imagery for 2005–2008, Vickery et al. (2013) noted high frequencies of dust plume activity over Etosha between June–

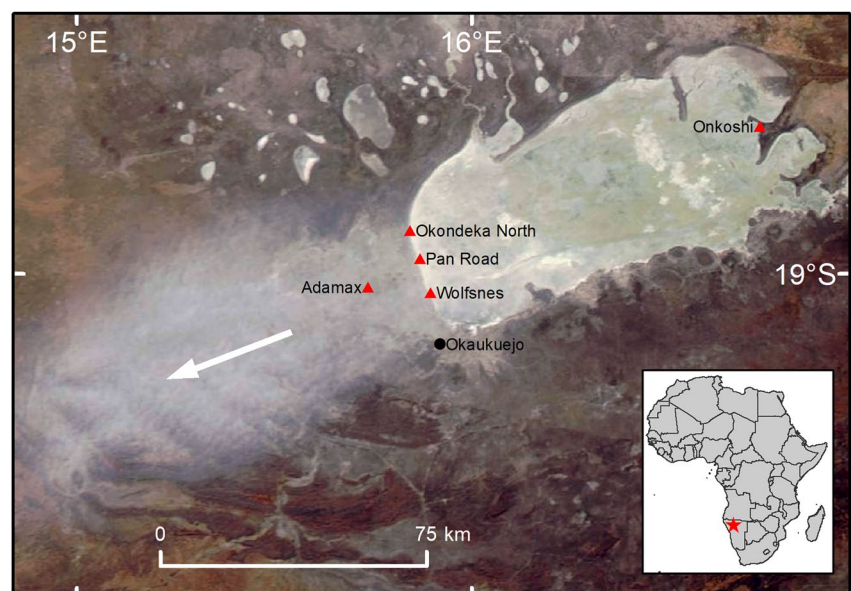


Figure 1. MODIS image of Etosha Pan in northern Namibia highlighting the location of the five monitoring stations located near named watering holes. The stations at Onkoshi (control), Okondeka North, Pan Road, and Wolfsnes collected data from July–September 2015, while the station at Adamax collected data for a full annual cycle until July 2016. A Halo Photonics doppler lidar was located at Okaukuejo. This Aqua MODIS scene was retrieved by a 1220 UTC overpass on 2 August 2015 during a measured dust emissions event blowing toward the south-west (bearing 069°), as evidenced by the gray emissions plume (see arrow). This event was recorded at all the western (downwind) stations and was ranked the third largest event in terms of horizontal dust flux (206.9 g/m²) during the entire observation period. The event comprised a peak measured aerosol concentration of 3.41 mg/m³ in response to a maximum wind velocity (*u*) at 3.18 m height of 9.81 m/s.

September with a peak in activity in the period June–August, responding in part to changing hydrological controls on surface erodibility (Bryant, 2003).

This recognition of variability in the frequency of dust emission events, and the seasonal dynamics in the dust cycle at Etosha Pan, has allowed a stronger comprehension of the likely broad-scale relationships between dust emission processes and their environmental controls. However, the extremely limited ground-based observations of climatic (especially wind power, erosivity) or surface (erodibility) drivers relevant to dust emission at Etosha Pan have prevented further understanding or quantification. Two field studies have sampled sediments from the surface of Etosha Pan to determine the possible influence of dust plume geochemistry and nutrient content on regional terrestrial and marine ecosystems west of the pan (Bhattachan et al., 2015; Dansie et al., 2017, 2022). However, no other surface or erodibility measurements relevant to aeolian dust emission from Etosha Pan are available in the literature.

More, but partial, ground-based data are available concerning the local boundary layer climate associated with dust emissions from Etosha Pan. The SAFARI observation campaign, focusing on biomass burning and ozone over southern Africa in 1992, included limited meteorological measurements using near-surface anemometers and balloon radiosondes at Okaukuejo, on the south-west edge of Etosha Pan (Figure 1; Zunckel, Held, et al., 1996). Observations in September and October 1992 identified a diurnal oscillation in winds over Etosha Pan with synoptically-forced E-NE winds during the day associated with the continental sub-tropical high, and lower velocity southerly winds at night resulting from a more local thermo-topographic forcing (Preston-Whyte et al., 1994). Data from the same field campaign also noted the existence of a frequent night-time temperature inversion and the associated development of a low-level jet (LLJ; Zunckel, Hong, et al., 1996). The existence of a nocturnal LLJ at Etosha Pan was recently confirmed by Clements and Washington (2021) using Doppler lidar. In this latter study the measured LLJ displayed characteristics of a strong, easterly wind (core windspeeds of around 12 m/s) strengthening to a maximum between 0600 and 0800 local time at a height of between 150 and 300 m. After sunrise, Clements and Washington (2021) noted that the breakdown of the LLJ resulted in strong surface winds between 0900 and 1100 local time which were associated with dust emission events observed during the months of August and September. LLJs have previously been associated with significant dust uplift in the Bodélé depression (Washington & Todd, 2005) and in the central Sahara and west Africa (Allen et al., 2013, 2015; Allen & Washington, 2014; Caton Harrison et al., 2019; Kaly et al., 2015; Marsham et al., 2013; Rajot et al., 2008).

3. Instrumentation and Methods

In order to fulfill our objective and obtain a comprehensive data set from which the controls, dynamics, and a quantification of the annual cycle of dust emission events could be determined, we established a network of meteorological and dust concentration monitoring stations at Etosha Pan for a period of 12 months, from 1st July 2015 to 30th June 2016. Five monitoring stations (Figure 1) were installed to provide measurements at (a) one control station at the eastern edge of the pan (Onkoshi), (b) three stations at the western edge of the pan (Okondeka North, Pan Road, Wolfsnes) along an 18 km transect perpendicular to the known and predominant W-SW heading of dust plumes (Vickery et al., 2013), and (c) a station in the center of the known dust plume trajectories (Adamax) 15 km west of the pan edge. Measurements at these stations (from 1st July to 23rd September 2015) covered the expected dust season in the austral winter, as recognised from previous remote sensing analyses (Bryant, 2003; Bryant et al., 2007; Vickery et al., 2013). The station at Adamax continued measurement until 30th June 2016 so providing data on dust event characteristics during the more humid summer months. These data from Adamax, measured outside of the recognised dust emissions season, permitted the first assessment of the complete annual dust cycle at Etosha Pan.

At each monitoring station a meteorological mast was erected (Figure 2) consisting of a Vector Instruments A-100LK cup anemometer and a Vector Instruments W-200P wind vane, both positioned at a height of 3.18 m. These instruments were logged at an interval of 10 min by a Campbell CR1000X datalogger. Additional instrumentation was deployed at Onkoshi, Wolfsnes, and Adamax including a Campbell Scientific CS215 temperature and relative humidity probe at 0.89 m, and a surface mounted tipping bucket raingauge.



Figure 2. A typical monitoring station (Pan Road) showing a 6 m anemometer tower on the left and a TSI DustTrak DRX aerosol monitor on the tripod in the center-right. All instrument data were logged at an interval of 10 min.

For each 10-min logging period the wind velocity (u) measured at a height of 3.18 m was used to calculate the Dust Uplift Potential (DUP), an indicator of the power of the wind available for generating dust emission in excess of the critical threshold for erosion, u_t (Bergametti et al., 2022; Marsham et al., 2011):

$$\text{DUP} = \left(1 + \frac{u_t}{u}\right) \left(1 - \frac{u_t^2}{u^2}\right) \text{ for } u > u_t; \text{ otherwise } 0$$

u_t was determined as described below and was considered constant throughout the entire annual measurement period. Whilst not reflecting dynamic changes to erodibility, as discussed by Bergametti et al. (2022), the assumption of a constant u_t allows the role of the erosive power of the wind (erosivity) in dust uplift to be isolated from that of changes in the susceptibility of the surface to erosion (erodibility). The total erosive power evident in each individual month during the measurement period was determined by summing each 10-min value of DUP.

Aerosol concentration was measured at each station using a TSI DustTrak DRX aerosol monitor (Wang et al., 2009; Watson et al., 2011) mounted on a tripod at 3.18 m height (Figure 2). This instrument recorded average concentrations (mg/m^3) of Total PM (equivalent to PM_{15} , referred to here as PM_{tot}) at 10-min intervals throughout the course of the field deployment. In order to specifically identify dust emission events originating from the pan, and to account for any aerosols advected across the pan from other upwind sources (e.g., regional dust haze), the aerosol concentration data from the eastern control station at Onkoshi were subtracted from all data measured at the western stations up to 23rd September 2015. For the remaining 9-month period of the study, when only the station at Adamax was deployed, no control data were available. However, outside of the dry winter period background levels of dust were negligible, averaging $0.012 \text{ mg}/\text{m}^3$ at Adamax during this 9-month measurement phase (see Figure 4).

There is no established protocol by which dust emission “events” should be defined using aerosol concentration data. In this study, discrete events were identified in the measured data where the 10-min average PM_{tot} aerosol concentration at any one of the western monitoring stations exceeded a value of $0.5 \text{ mg}/\text{m}^3$. This threshold concentration value is a conservative identifier for an event as it lies qualitatively between values representing “severe haze” and “moderate dust storm” classes used by Leys et al. (2011). However, Leys et al. (2011) employed hourly averages (rather than the 10 min applied here) and were measuring at considerable distance from the emissions source. Based on measurements made directly at an emitting surface, Mockford et al. (2018) reported a value of $0.25 \text{ mg}/\text{m}^3$, also over an hour average period to define dust events in Iceland, using a DustTrak at 1.4 m

height. Of note is that the events identified using the 0.5 mg/m^3 threshold in the austral winter (July–September) qualitatively match with those observed using remote sensing imagery (e.g., Figure 1). The analytical boundaries employed here for identifying individual events are therefore considered practical and allow reasonable comparison with other studies of dust emission where aerosol concentration has been measured on an event basis across a variety of averaging times and at widely varying distances from source (e.g., Bergametti et al., 2018, 2022; Draxler et al., 2001; Gong & Zhang, 2008; Kaly et al., 2015; Klose et al., 2019; Lee et al., 2009; Marticorena et al., 2017; Rajot et al., 2008; Wang et al., 2008).

In the absence of direct measurements of dust emission from the local surface, the relative magnitude of measured dust events was quantified by calculating a derivative of horizontal dust flux ($\text{mg/m}^2/\text{s}$) from the factor of windspeed (m/s at 3.18 m height) and the co-located aerosol concentration measurements (PM_{tot}), giving a total horizontal flux aggregated over the 10 min logging period ($\text{g/m}^2/\text{min}_{10}$) at 3.18 m height. For each discrete dust emission event, all the 10-min horizontal fluxes occurring within the event were summed for the measured event duration. This procedure therefore determined the total mass of sediment (g/m^2) transported horizontally during each individual event at 3.18 m height, termed the *event flux*. It should be noted that the event flux does not reflect the complete horizontal mass of sediment transported during each dust event as such an assessment also requires full characterization of event plume width and height, inclusive of the attenuation in horizontal flux with height. Such calculations require significant assumptions and include large uncertainties (see Leys et al., 2011; Todd et al., 2007). With the data available, the analysis presented here provides a reasonable quantification of the relative magnitude of each measured event using measured and defined quantities (*horizontal dust flux* and *event flux*) that are distinct from *vertical dust flux*, as resolved in some other studies (e.g., Webb et al., 2021; Zobeck & Van Pelt, 2006).

The measurements of 10-min aerosol concentration for each identified event ($>0.5 \text{ mg/m}^3$) at the sites on the western edge of the pan (Okondeka North, Pan Road, Wolfsnes; Figure 1) were used to calculate a probability distribution of critical windspeeds (u_c at 3.18 m height) that were associated with the occurrence of dust events. This was accomplished by identifying the measured value of u coincident with measurements of PM_{tot} reaching above background levels on the rising limb of each recognised dust event. The measurement sites were located at the western edge of the eroding pan surface so the calculated erosion threshold offers only an indefinite indication of actual threshold values at the local source of emission. However, given that the specific source of each dust emissions event can differ markedly across the pan (Bryant, 2003), the calculation of a critical erosion threshold here provides the best available quantification.

A Halo Photonics Streamline Pro Doppler lidar was installed at Okaukuejo on the south-west edge of the pan (Figure 1) for the period 4th July to 23rd September 2015. The lidar returned boundary layer profile measurements at heights $>30 \text{ m}$ above the surface of aerosol backscatter and vertical windspeed every 2 s, as well as horizontal wind speed and wind direction every 15 min at a 3 m vertical resolution for the duration of its deployment. For subsequent data analysis the 2 s-frequency aerosol backscatter and vertical velocity measurements were averaged over 1 min intervals. However, the positioning of the lidar on the SW edge of the pan resulted in the instrument under-recording the frequency of dust events observed at the other monitoring stations by around 50%. This was because the trajectory of many of the dust plumes was located north of the lidar deployment site. Further, for all the remaining events that were detected by the lidar there was a significant attenuation in signal with height, limiting useable data to below around 0.6–1.2 km in height. Similar attenuation effects have been experienced elsewhere where lidar has been deployed for aerosol detection (Allen et al., 2013).

4. Results and Discussion

4.1. Annual Dust Event Dynamics

Analysis of the annual wind regime during the study period showed a bimodality in the predominant winds (Figure 3a). The highest frequency winds originated from the SW (190° – 210°) reaching maximum values $<7.5 \text{ m/s}$. However, the strongest winds were seen from the ENE (60° – 80°) with reasonably frequent winds $>7.5 \text{ m/s}$, peaking at 16.81 m/s. These annual measured data correspond to the shorter-term wind observations for the region noted by Zunckel, Held, et al. (1996) and Preston-Whyte et al. (1994) referred to above.

The strong ENE winds were responsible for dust emission from the pan surface during the study period, with data on both total aerosol concentration (Figure 3b) and horizontal dust flux (Figure 3c) showing a very strong

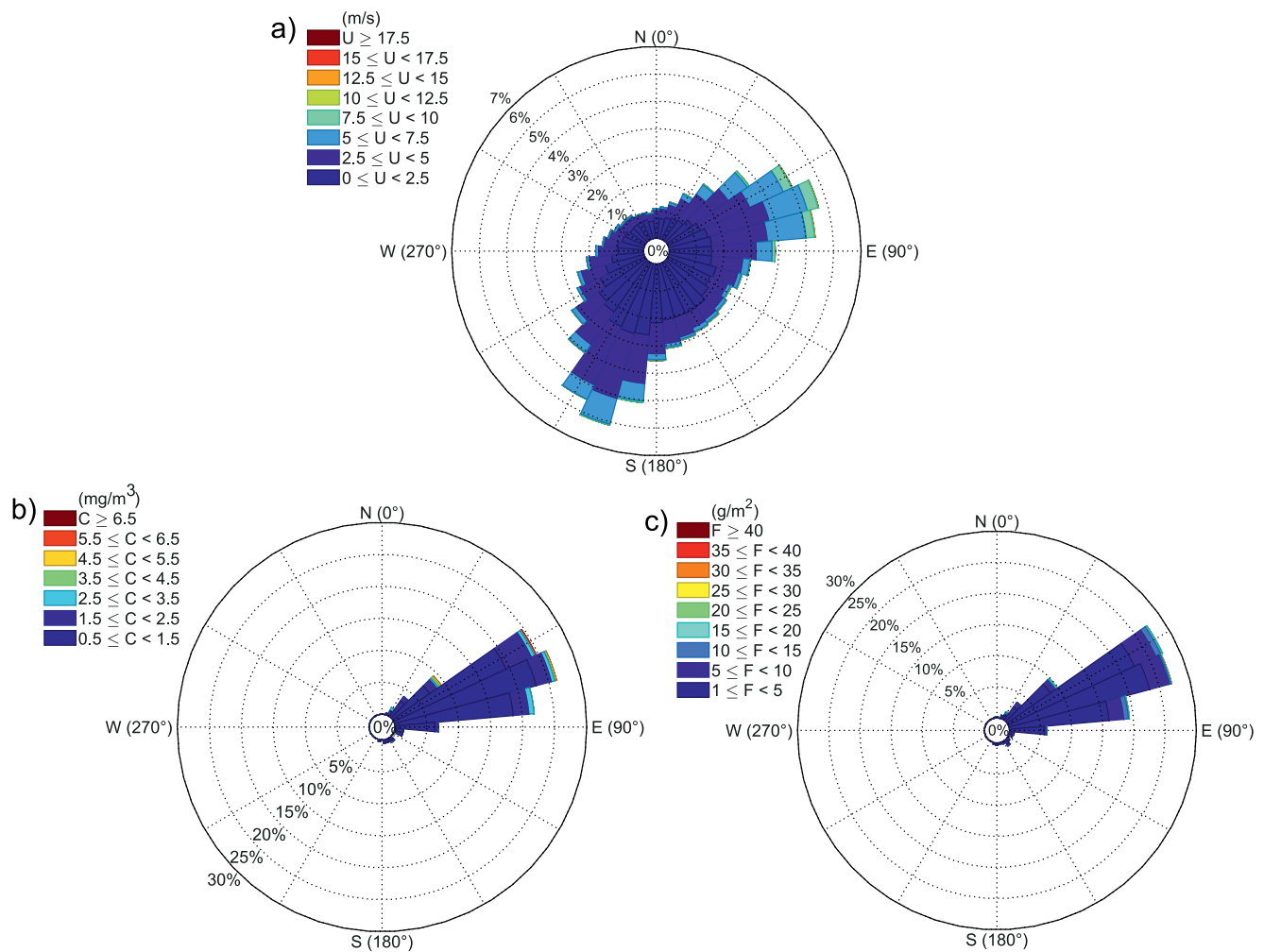


Figure 3. Annual wind and aerosol statistics measured at Adamax, 1st July 2015–30th June 2016. (a) Wind velocity measured at 3.18 m height (u , m/s); (b) aerosol concentration (mg/m^3); (c) calculated horizontal dust flux (g/m^2).

directional orientation between 60° and 80° . Given the positioning of the sampling equipment on the western edge of the pan, where the pan is the principal source of erodible sediment, this directional relationship between wind and dust flux is unsurprising. However, these field data correspond to previous remote sensing studies which have also identified this directional predominance in dust plume development from Etosha Pan (Bryant et al., 2007; Vickery et al., 2013). Further, there was no evidence in the data collected at Onkoshi, at the eastern edge of the pan, that dust uplift occurred in response to any of the frequent SW winds. Data in Figure 3 indicate that these SW winds only infrequently exceeded the calculated threshold for erosion of the pan surface (modal $u_t = 7.25$ m/s), whilst the ENE winds surpassed these thresholds to a far greater degree and were principally responsible for observed dust emission.

Examination of the measured aerosol concentrations identified 51 significant dust emission events where average PM_{tot} aerosol concentration values exceeded the selected $0.5 \text{ mg}/\text{m}^3$ threshold (Figure 4). Emission events occurred throughout the annual cycle but large events with higher peaks in aerosol concentration were notably more prevalent in the first half of the measurement period (July–December 2015). The largest event in terms of peak aerosol concentration occurred on 5th November 2015 where average 10-min values reached a maximum of $6.04 \text{ mg}/\text{m}^3$ (Figure 4). This order of magnitude for dust event aerosol concentration is comparable to that measured in the western Sahara by Marticorena et al. (2017) who recorded a 5-min maximum (PM_{10} concentration) of $24.7 \text{ mg}/\text{m}^3$ in Mali during the most intense dust event they observed over a 6-year period, Zhang et al. (2018) who observed a maximum hourly concentration of $42.7 \text{ mg}/\text{m}^3$ in Inner Mongolia, a $33.9 \text{ mg}/\text{m}^3$

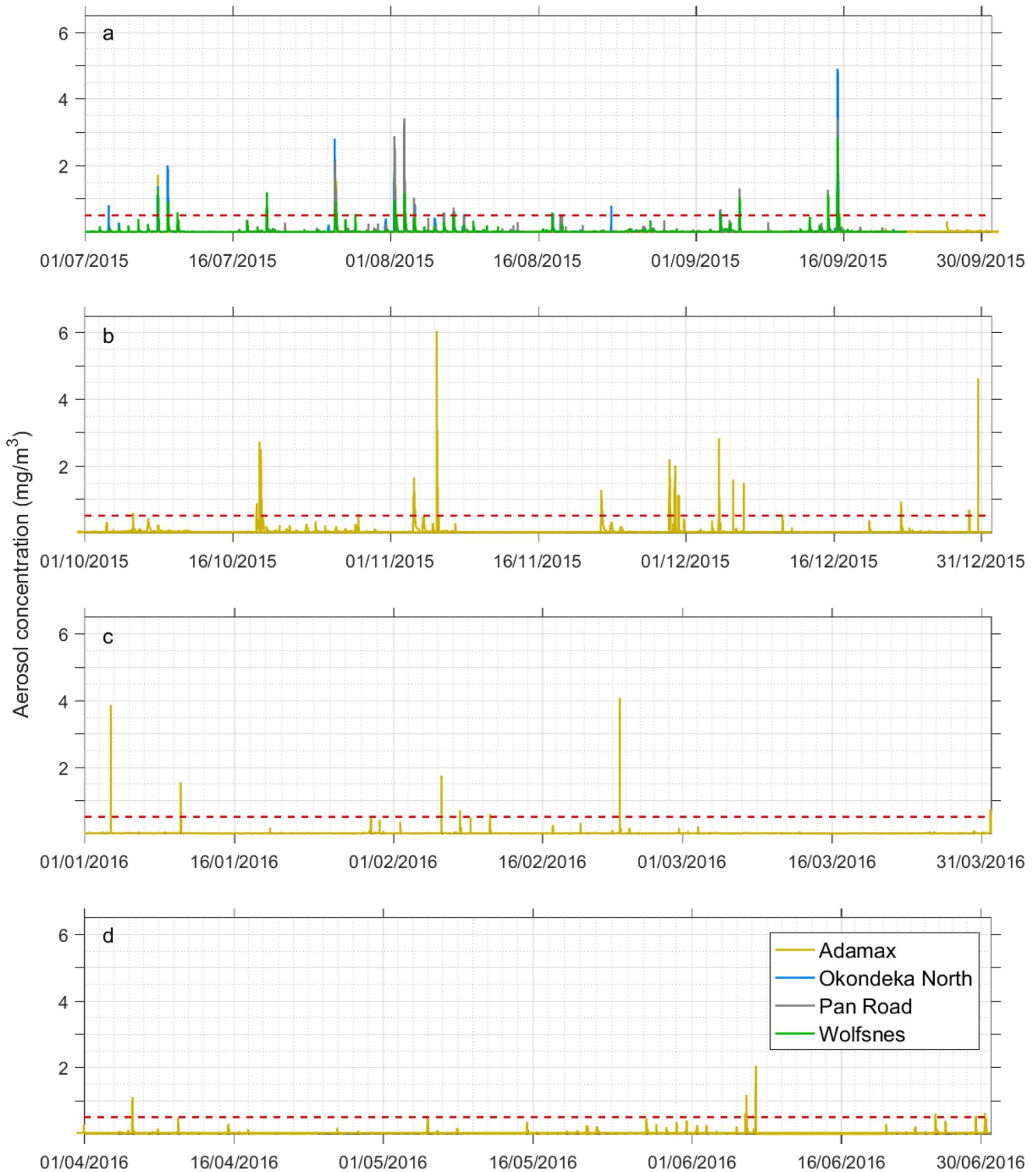


Figure 4. Time series of measured aerosol concentration (PM_{10} , mg/m^3) throughout the full experimental period for the four monitoring stations at the west of the Pan. The horizontal red dashed line indicates the threshold used to identify individual dust events, where measured aerosol concentration exceeded $0.5 mg/m^3$ ($n = 51$). (a) July–September 2015, (b) October–December 2015, (c) January–March 2016, (d) April–June 2016.

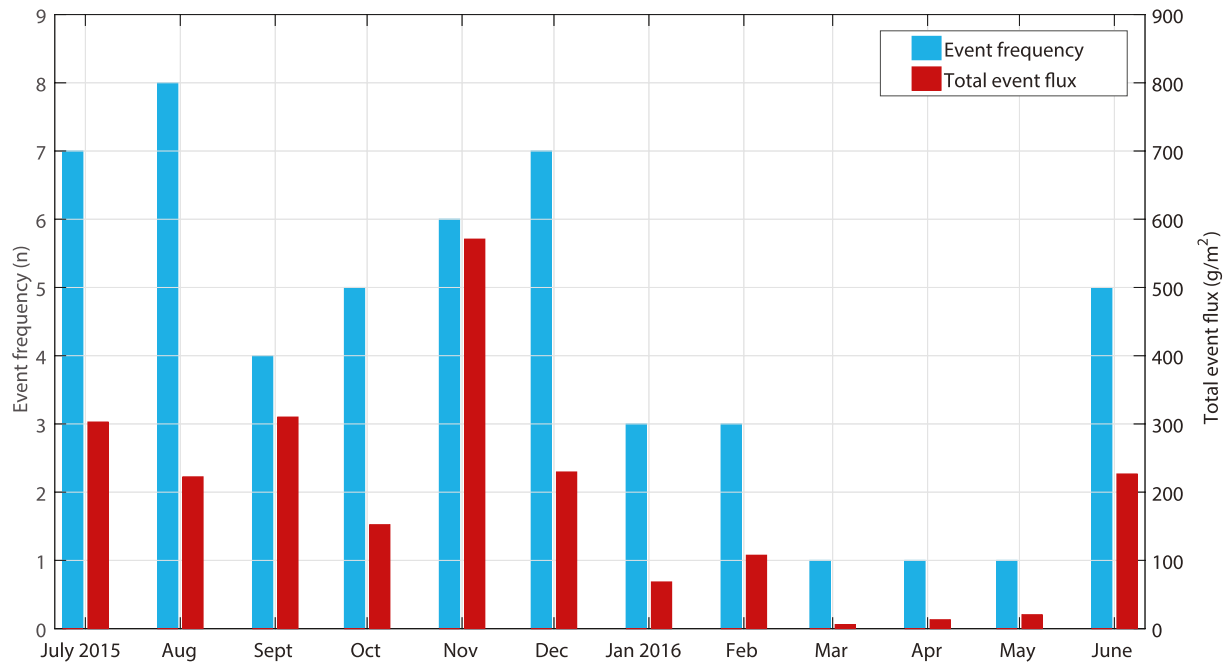


Figure 5. Observed frequencies of dust events and monthly totals of event flux. These ground-based data reveal a new quantitative understanding of dust event frequency and magnitude at Etosha Pan. Whilst the frequency of events is greatest in the winter (July and August), the relative magnitude of dust events (i.e., total event flux) is greatest in the spring (November). These field data also highlight the magnitude of dust events in the austral spring and summer (October to February) which has previously gone unrecorded by remote sensing observation.

aerosol concentration measured over 5 min during a dust storm in southern Tunisia (Bouet et al., 2019), and an hourly average of 15.39 mg/m³ measured by Leys et al. (2011) during the 2009 “Red Dawn” event in SE Australia. Whilst comparison between the data we present here and previous studies is useful for context, it should be noted that each of these cited experiments employed differing measurement methods, durations, and experimental designs and so data are not directly comparable.

The annual distribution of the 51 identified dust events (Figure 5) shows the expected winter (July–September) peak in frequency ($n = 19$), in broad agreement with findings from previous remote sensing investigations

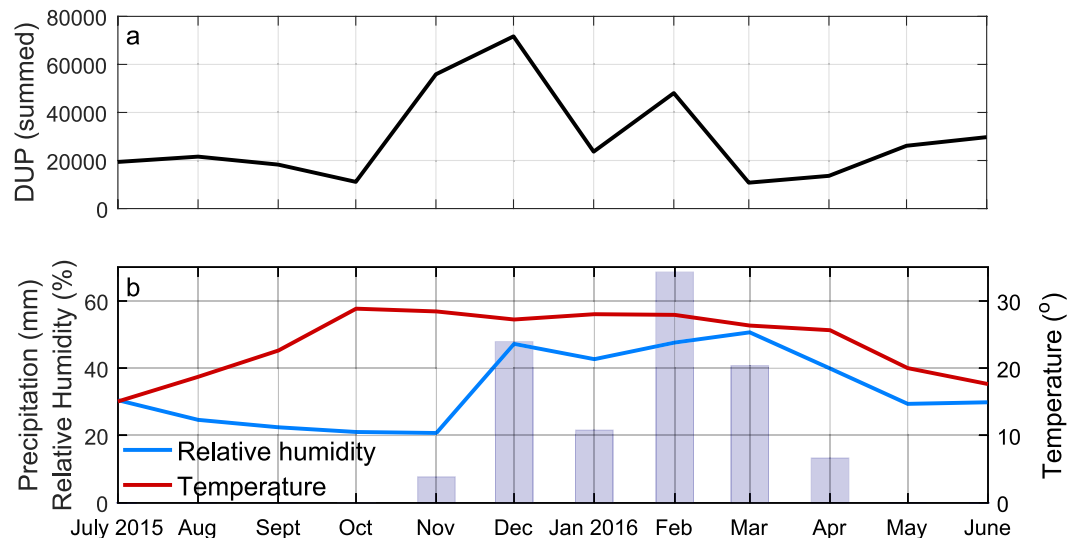


Figure 6. Key meteorological variables associated with (a) wind erosivity (Dust Uplift Potential (DUP) summed for each month) and, (b) surface erodibility. Bars represent precipitation.

(Bryant, 2003; Vickery et al., 2013). Critically, however, the measured data here also indicate the unexpected persistence of dust events throughout the austral spring and summer. This is in stark contrast to previous remote sensing studies (Bryant, 2003; Bryant et al., 2007; Vickery et al., 2013) which have not observed dust emissions outside of the winter season. Our ground measured data reveal a total of 21 events during October–January including seven in December alone. It is not until March–May 2016 that the observed frequencies of dust events reduce to low levels, before increasing again in June.

4.2. Dust Event Response to Changing Erosivity and Erodibility Conditions

The measured field data allow us to explore not only the frequency of dust events but also the relative magnitude of the events, in the context of the mass of sediment (g/m^2) transported during each event (the event flux), summed to provide a total event flux for each month (Figure 5). This metric offers a better quantification of the contribution of dust events to atmospheric dust loading than static measurements of aerosol concentration as it accounts for the varying windspeed and total duration of each event. In contrast to the frequency analysis of dust events (based on aerosol concentration measurements) which broadly recognised the winter months (July–August) as the most significant for dust activity, Figure 5 shows a very clear peak in total event flux during November. In this month, the six recognised events generated a total event flux of $571 \text{ g}/\text{m}^2$, more than double the average winter monthly (July–September) event flux of $279 \text{ g}/\text{m}^2$.

The rapid increase in event flux in November appears to be controlled by a changing and complex pattern of erosivity (wind power) and surface erodibility (susceptibility to erosion) conditions in the transition period between the dry winter and wetter summer months. Figure 6a reveals that November 2015 was characterized by significantly increased erosive potential, illustrated by steeply rising values of DUP throughout November toward a peak in December. This increased erosivity in November coincided with strongly desiccating conditions of negligible precipitation (7.7 mm), a minimum in mean RH (20.74%), and high mean air temperatures (28.45°C) (Figure 6b). Such desiccating conditions are known to increase surface erodibility on evaporative pan surfaces of this type (Nield, McKenna Neuman, et al., 2016) with evidence suggesting that over several months they can encourage an increase in the supply of fine sediment as pan surfaces crack and degrade (Haustein et al., 2015; Nield et al., 2015; Nield, Wiggs, et al., 2016). Whilst the specific relationships between erosivity and erodibility will vary year to year, in the case of dust emissions on Etosha Pan in 2015, it appears that the erosivity and erodibility conditions in the austral spring (November) resulted in fewer but higher magnitude events (in terms of horizontal flux) than the preceding winter months of July and August (Figure 5). It is the winter months that are more commonly considered as comprising the dust season (Bryant et al., 2007; Vickery et al., 2013) and the analysis here illustrates the very different dust event dynamics that can be interpreted via a distinction between dust event frequency and horizontal dust event flux.

The erosive potential of the Etosha aeolian system, evaluated by calculations of DUP, peaks in December and remains at intermediate to high levels in the remaining summer months of January and February (Figure 6a). These higher levels of erosivity in the summer are likely associated with the development of convective systems (Engert, 1997; Mendelsohn et al., 2013). However, this erosive potential is largely counteracted by reductions in erodibility of the surface driven by the effects of high precipitation (Dec-Feb total of 138 mm, leading to pan surface wetting) and high relative humidity (RH, $\sim 47\%$). Such high values of RH have been shown to reduce observed aerosol concentrations elsewhere (Csavina et al., 2014). These drivers of low surface erodibility give rise to declining levels of dust event frequency and dust event flux throughout January and February (Figure 5). The austral autumn shows further reductions in dust event flux (Figure 5) with declining levels of DUP, especially in March (Figure 6a) where precipitation totals remain significant (40.8 mm) and RH values remain high ($\sim 50\%$). The period of higher aeolian dust fluxes evident in the months of June to September (Figure 5) appears to be controlled by increasing surface erodibility (including, in years with pan inundation, the recession of surface flooding; Bryant, 2003) through desiccation. This is seen as a response to a rising mean temperature and a continuous decline in RH after the summer rains (Figure 6b), more than any significant increase in erosivity potential as defined by the DUP (Figure 6a). During these winter months DUP is seen to increase from the minima in March and April but remains largely stable (Figure 6a).

The critical significance of changing surface erodibility in controlling dust event dynamics on Etosha Pan, as discussed above, highlights the necessity for high resolution surface erodibility data at the exact locations of

dust emission. The lack of such data continues to act as a first-order limit to our knowledge of the controls on emissions processes (Klose et al., 2019), especially on crusted surfaces. Gaining such data is challenging because specific dust emissions sources are dynamic and heterogenous in both space and time (Bryant, 2003; Haustein et al., 2015), and are especially sensitive to the local formation and breakdown of surface crusts (Nield et al., 2015; Nield, McKenna Neuman, et al., 2016). Whilst the measurements presented here offer an insight into likely major controls on surface erodibility of air temperature, RH, and precipitation, additional data specific to the precise emitting surfaces would offer a far more robust comprehension (Csavina et al., 2014; Goldstein et al., 2017).

4.3. Dust Event Dynamics and Forcing Mechanisms: Low-Level Jets and Cold Pool Outflows

Analysis of the 51 recognised dust events measured over the entire year allows the identification of their characteristics at the event scale. Figure 7 clearly identifies a bimodality in the distribution of events distinguished using measurements of the event start time (hours after sunrise) and the total duration of the event. In the context of start time, events were initiated either in the morning, within 0.5–5.0 hr after sunrise (peak frequency at 3.0–4.0 hr), or much later in the day with a wide distribution of start times between 10.5 and 16.5 hr after sunrise. These later times equate to emissions being generated around sunset and into the late evenings up to 2230 hr local time. The data in Figure 7 also demonstrate a pattern in the duration of dust events with those initiated earlier in the day lasting anywhere between 40 and 420 min, and those initiating much later in the day, excepting one longer-lasting event, generally restricted to shorter durations of between 30 and 120 min. These later-starting events all occurred in the 6-month period between October and early April (Figure 7), principally coinciding with the start and end of summer rainfall (Figure 6). This general distinction between earlier/longer dust emission events in the winter, and later/shorter dust emission events in the summer points to two contrasting climatological mechanisms driving dust dynamics in these different seasons; the breakdown of low-level jets (LLJ) in winter mornings, and cold pool outflows (CPO) associated with evening convective storms in the summer. Each of the dust emission events was attributed to the most likely of these forcing mechanisms using the criteria described by Allen et al. (2013) and described in Text S1 and Table S1 in Supporting Information S1.

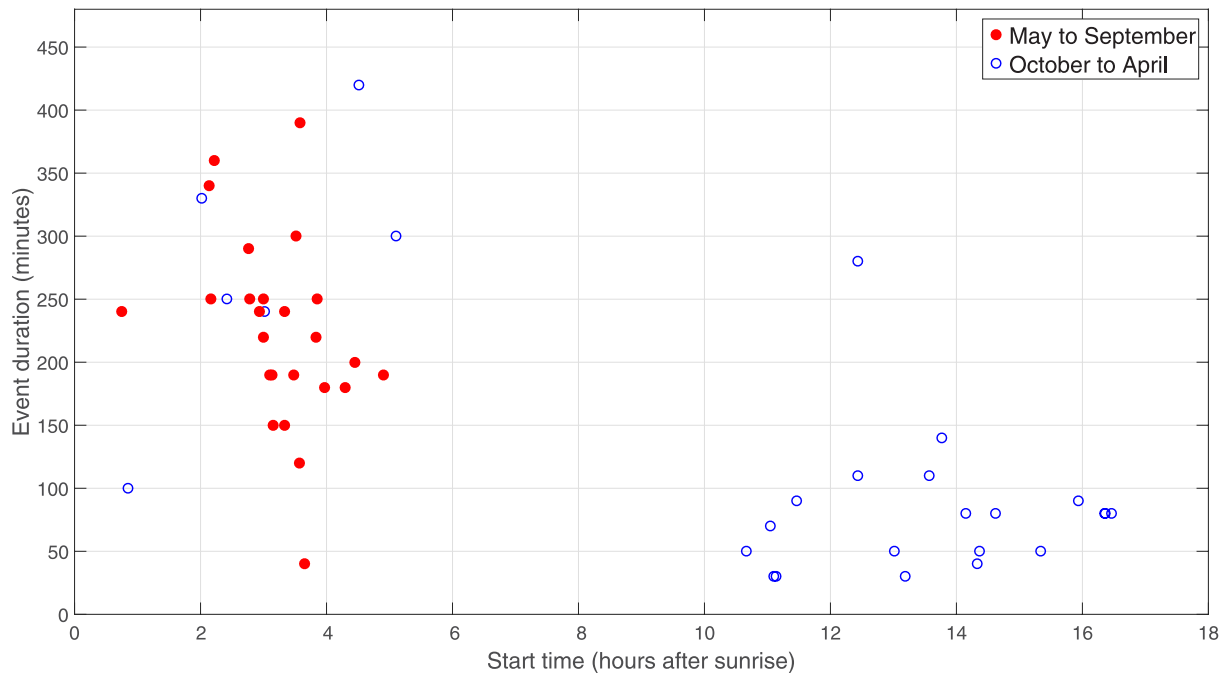


Figure 7. Dust events discriminated by measured start time (hours after local sunrise) and event duration (minutes). Dust events characterized by early start times and longer durations are considered to be driven by the breakdown of low-level jets in winter (dry season) mornings. In contrast, those dust events characterized by much later start times and shorter durations are interpreted to be a result of cold pool outflows in summer (wet season) evenings. Note that this seasonal distinction is somewhat obscured in the austral spring with 6 of the 11 events in October and November plotting on the left-hand side of this Figure.

The development of near-surface low-level jets associated with dust emissions has been investigated across the Sahara (Allen et al., 2013; Bergametti et al., 2018; Fiedler et al., 2013; Kaly et al., 2015; Marsham et al., 2013; Schepanski et al., 2009), in the Bodélé depression, Chad (Todd et al., 2007; Washington et al., 2006; Washington & Todd, 2005), and in the Taklimakan, China (Ge et al., 2016). There are also observations of the frequent occurrence of LLJs with an easterly component over Etosha Pan during winter months (Clements & Washington, 2021; Zunckel, Held, et al., 1996) when strong radiative cooling at night promotes the decoupling of air aloft from the surface and nocturnal stratification of the atmosphere (Allen & Washington, 2014; Blackader, 1957). Inertial oscillation leads to a nocturnal acceleration of the wind which is then mixed down to the surface following strong surface heating.

In cases where dust plumes tracked over the lidar during the monitoring campaign, data provide evidence supporting the operation of a LLJ-driven dust emission mechanism during dry winter months, supporting the findings of Clements and Washington (2021). Figure 8 presents data on horizontal wind speed and aerosol backscatter from the lidar together with SEVIRI satellite data over a period of 3 days (8th, 9th, and 10th July 2015) for a series of medium intensity dust events. On each of these days a jet of fast-moving wind in excess of 9.0 m/s was established around 300–500 m above the ground in the early morning between 0600 and 0900 hr (Figure 8a). After sunrise (at 0630 hr), the onset of radiative heating is seen to drive vertical mixing of the wind profile (Allen & Washington, 2014; Clements & Washington, 2021), conveying the fast-moving winds at altitude toward the surface as the elevated LLJ breaks down and becomes absorbed into the synoptically-forced gradient wind (Zunckel, Held, et al., 1996). Between 0900 and 1000 hr these high-velocity horizontal winds are seen to have reached the pan surface resulting in the erosion of surface sediments, driving peaks in aerosol backscatter as measured by the lidar 1–2 hr later (Figure 8b). The resulting south-westerly tracking dust plumes can be seen in the SEVIRI satellite data (Figure 8c).

The surface impact of this LLJ-driven dust emission mechanism is clearly recognizable in the ground-based data from those measurement stations on the edge of the pan, sited immediately downwind of emitted dust plumes. Figure 9a presents these data for a typical event that occurred on 2nd August 2015. The data demonstrate low overnight surface wind speeds until around 0800–0900 hr, after which they steadily increased in response to vertical atmospheric mixing driven by a rising air temperature (notable from around 0700 hr with sunrise at 0624 hr, Figure 9a). In the 40 min between 0910 and 0950 hr the mixing of fast-moving air down to the surface as the LLJ collapsed into the gradient wind resulted in values of windspeed (measured at 3.18 m) rising from ~3.00 m/s to a maximum of 9.81 m/s. This is well in excess of the modal threshold value for erosion calculated as $u_t = 7.25$ m/s. This dramatic increase in erosive force resulted in erosion of the pan surface sediment leading to a rapid rise in measured aerosol concentration to a peak of 3.41 mg/m³. Aerosol concentrations then declined to pre-event levels by 1400 hr (a 290 min event duration), in association with weakening windspeeds throughout the rest of the day.

The progressive increase in the wind velocity time series in the hours after sunrise, shown in Figure 9a, has been demonstrated as characteristic of the process of mixing-down of LLJ structures in the central Sahara (Allen & Washington, 2014; Washington et al., 2006). This process is typified by a strong rise in surface windspeed within 1–5 hr after sunrise (Caton Harrison et al., 2019; Parker et al., 2005) reaching a peak in mid-morning, followed by a slow decline to mid/late afternoon, and has been noted in measurements of the Bodélé LLJ by Washington et al. (2006) in Chad, and observations in the central Sahara as part of the FENNEC campaign by Allen et al. (2013) and Marsham et al. (2013). In both regions, the development and subsequent breakdown of LLJs are recognised as a principal mechanism for dust raising. It is notable that Clements and Washington (2021) identify the morning development of LLJs on >90% of days during their study at Etosha Pan, with strong LLJ structures associated with all six of their detected dust emission events.

The 31 dust emission events attributed to the LLJ process in this study (see Supporting Information, Table S1) accounted for 61% of all the events observed over the annual cycle. This proportion is comparable to that estimated over the Bodélé from analysis of model data (Fiedler et al., 2013).

In the summer period from early December to April, we found no evidence of the breakdown of a LLJ increasing surface windspeeds and resulting in dust emission. As noted by Allen and Washington (2014), the development of LLJs is favored by conditions of strong synoptic-scale pressure gradients and, at Etosha, these are found in winter with high pressure circulation persisting over southern Africa (Tyson & Preston-Whyte, 2015). Rather, between October and April (and exclusively from early December) the Cold Pool Outflow (CPO) mechanism was

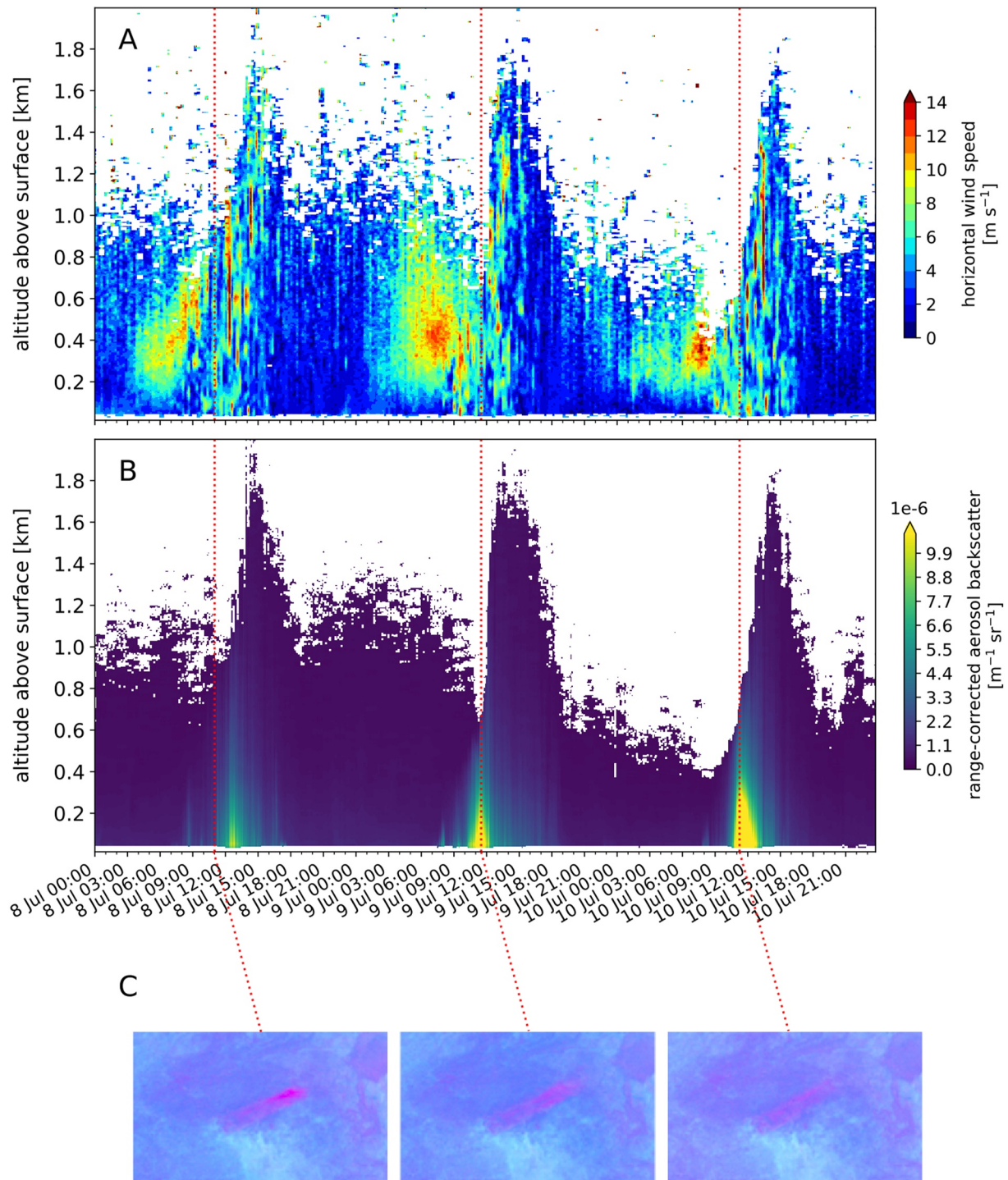


Figure 8. Doppler lidar data (instrument located at Okaukuejo, see Figure 1) and SEVIRI remote sensing imagery for consecutive dust emission events occurring on 8th, 9th and 10th July 2015. (a) Vertical profile of horizontal windspeed, white areas signify signal attenuation; (b) vertical profile of aerosol backscatter; (c) SEVIRI image of northern Namibia showing dust plumes in pink tracking south-west from Etosha Pan, similar to the true-color image in Figure 1.

observed to dominate dust emission processes in the summer evenings (see Table S1 and Figure S1 in Supporting Information S1, and Figure 7). Developing as convective downdrafts from deep convection, CPOs have commonly been recognised as a major cause of dust emissions (Allen et al., 2013; Kaly et al., 2015; Knippertz

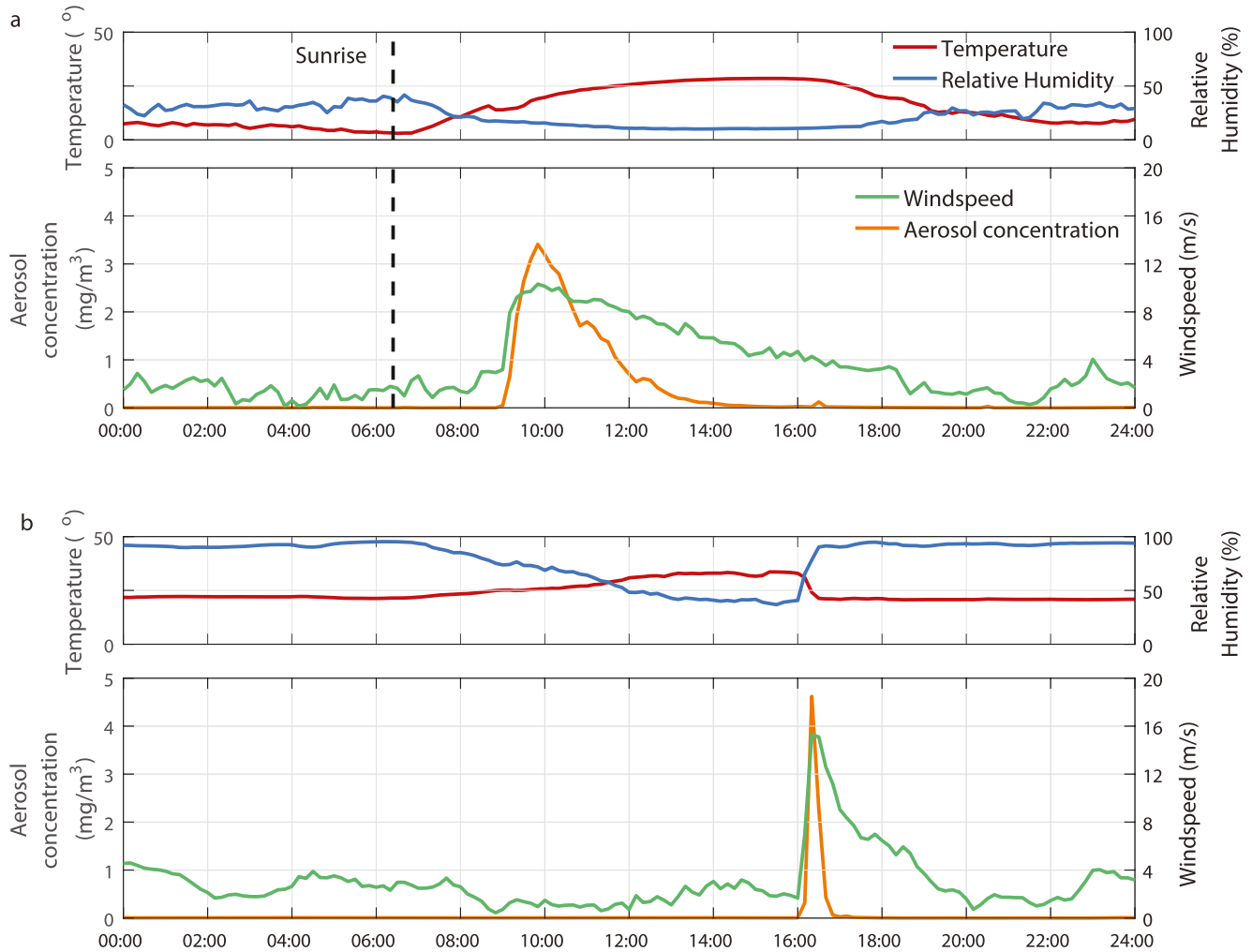


Figure 9. Surface measurements of aerosol concentration and boundary layer climate during, (a) a typical Low Level Jet-driven dust emission event on 2nd August 2015 and, (b) a typical Cold Pool Outflow-driven dust emission event on 30th December 2015.

et al., 2007; Marsham et al., 2008) capable of generating high velocity surface winds (Marsham et al., 2013; Sow et al., 2009).

An example of a typical CPO-driven emission event over Etosha Pan is detailed in Figure 9b. This event occurred on 30th December 2015 when high air temperatures in the afternoon (mean 33°C) generated the development of a convective storm cell (clearly visible in coincident SEVIRI satellite images, see Figure S1 in Supporting Information S1), evidenced by a rapidly rising RH from 40% to 90% at 1600 hr, and an associated decline in temperature to 21°C. Such sudden changes in humidity and temperature are characteristic of cold pool activity (Bergametti et al., 2022; Emmel et al., 2010; Marsham et al., 2013; Provod et al., 2016) and the outflow of air associated with the development of the convective cell rapidly generated highly erosive winds (Allen et al., 2013, 2015; Miller et al., 2008). Within 30 min the measured windspeed at 3.18 m height rose from ~2.00 m/s to a maximum of 15.28 m/s. This resulted in significant erosion of the surface sediments and a peak aerosol concentration of 4.62 mg/m³, representing one of the highest aerosol concentrations measured during the year-long experiment. In contrast to the LLJ mechanism, the erosive winds generated by the CPO dissipated quickly with aerosol concentrations returning to pre-event levels within 50 min (Figure 9b).

These developmental characteristics of CPO-driven dust emission, typified by very rapidly rising surface wind velocity resulting in significant generation of dust, are comparable to those measured by Sow et al. (2009) and Allen et al. (2013, 2015) in the Sahara, and Provod et al. (2016) and Bergametti et al. (2022) in the Sahel. At Etosha, our data demonstrate that 39% ($n = 20$) of all dust events (where aerosol concentration >0.5 mg/m³)

showed characteristics of being driven by the CPO mechanism (See Table S1 in Supporting Information S1). The short duration but high intensity dust emissions (See Table S2 in Supporting Information S1), and the presence of deep convective cloud associated with CPO-driven events, makes them difficult to detect from remote sensing observation (Allen et al., 2015; Caton Harrison et al., 2021). However, the recognition of CPOs driving dust emissions at Etosha and other sites of significant dust activity is important because the small-scale processes which generate them are not well constrained by emissions models (Bergametti et al., 2022), and so their contribution to total atmospheric aerosol load is therefore under-represented globally (Caton Harrison et al., 2021; Marsham et al., 2013).

4.4. Quantifying Dust Event Magnitude

The co-located ground measurements of 10-min wind velocity and aerosol concentration offer the opportunity to compare event magnitude in terms of the mass of dust (g/m^2) transported horizontally during the course of each of the identified dust events (the event flux). The total annual event flux for all 51 identified events summed during the experiment amounted to $2,919 \text{ g}/\text{m}^2$ (Table 1). This compares to the total annual flux, including aerosol measurements not specifically identified as an event, of $3,924 \text{ g}/\text{m}^2$.

These data highlight both the competence of winds at Etosha Pan to erode and transport substantial volumes of sediment annually, and also the significance of the 51 individual events which accounted for over 74% of total annual horizontal dust flux. Indeed, the largest six events in terms of event flux magnitude, accounting for around 12% of events by frequency, explained nearly 31% of the total annual horizontal flux (Table 1). This weighting toward the greater significance of higher magnitude events to the total mass of dust eroded and transported by wind at Etosha is shown in the power relationship recognised between event magnitude and frequency in Figure 10. Hence, although low magnitude events were of high frequency, total horizontal dust flux was dominated by a handful of very large events. The maximum recorded single horizontal event flux was $302 \text{ g}/\text{m}^2$ for a 340 min duration event which started at 0800 hr on 15/9/2015 (Table 1). This event was driven by high velocity winds (peaking at $u = 9.38 \text{ m}/\text{s}$) and showed characteristics consistent with the breakdown of a LLJ (Table S1 in Supporting Information S1). This single event accounted for nearly 8% of the total annual horizontal dust flux. The significance of low frequency but high magnitude events to annual statistics of a regional dust emissions budget are rarely reported, but assessments have previously been noted in the western Sahara by Marticorena et al. (2017) who recorded 47% of annual dust deposition occurring within a single event.

The top five highest values of event flux were represented by events characteristic of LLJ-driven erosion (see Table S1 in Supporting Information S1). Despite CPO-driven events recording higher average maximum wind speeds ($10.3 \text{ m}/\text{s}$) and constituting 39% of all recorded events by frequency, they accounted for only 16% of the total annual flux (Table 1). This compared to the more frequent (61%) LLJ-driven events with lower average maximum windspeeds ($8.8 \text{ m}/\text{s}$) which accounted for 58% of the total annual flux. This finding contrasts with investigations in the central Sahara where CPO-related emission events have been observed to dominate dust activity, accounting for up to 82% of dust plume frequency (Caton Harrison et al., 2019). The reduced

Table 1
Calculated Event Frequencies and Horizontal Dust Fluxes

	Count (n)	Calculated flux (g/m^2)	Proportion of recognised events by frequency (%)	Proportion of total annual flux (%)
Total annual flux ^a	–	3,924	–	100
Total annual non-event flux ^b	–	1,005	–	25.6
Total annual event flux ^c	51	2,919	100	74.4
Largest six events	6	1,209	11.8	30.8
Largest single event	1	302	1.9	7.7
Total LLJ-driven event flux	31	2,275	60.8	58.0
Total CPO-driven event flux	20	644	39.2	16.4

^aTotal flux calculated throughout the annual observation period (g/m^2). ^bTotal flux not in a specifically recognised emissions event (i.e., $\text{PM}_{\text{tot}} < 0.5 \text{ mg}/\text{m}^3$) (g/m^2). ^cTotal flux occurring in specific events where $\text{PM}_{\text{tot}} > 0.5 \text{ mg}/\text{m}^3$ (g/m^2).

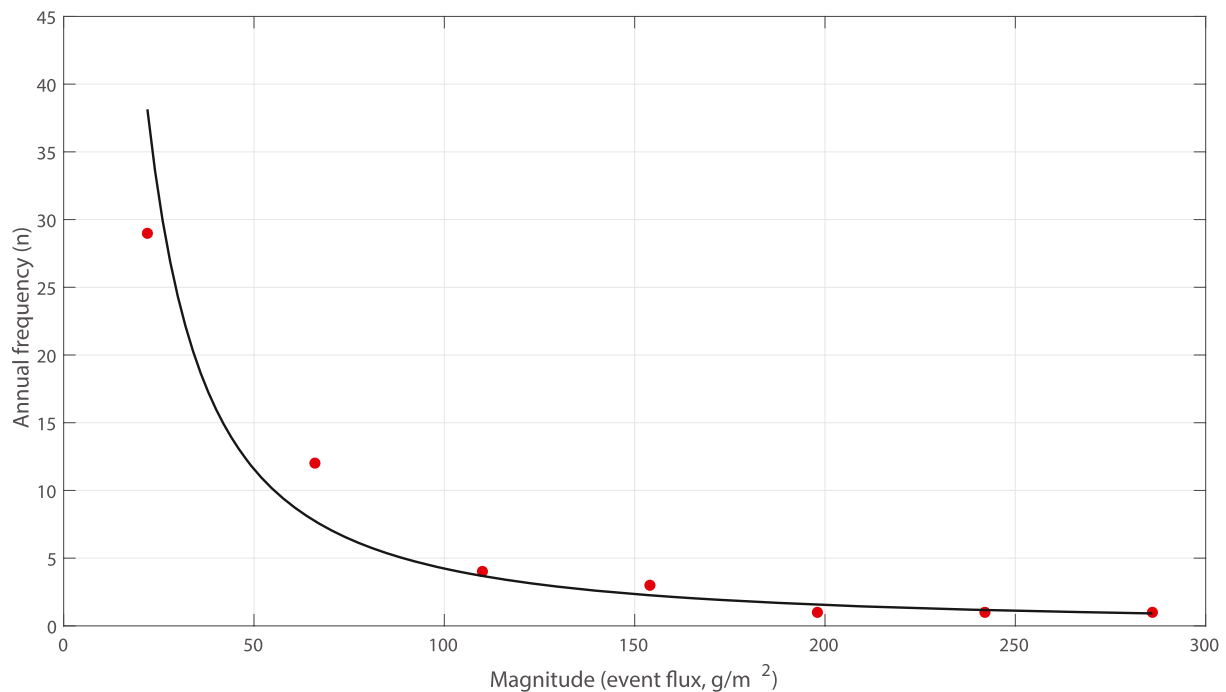


Figure 10. The magnitude-frequency relationship for dust events (where $PM_{10} > 0.5 \text{ mg/m}^3$) at Etosha Pan, July 2015–June 2016. Event flux data plotted at the mid-point of bins of equal width (44 g/m^2).

significance of CPO-driven events at Etosha may be explained by their occurrence being restricted to the summer when the erodibility of the pan surface is much reduced by ephemeral flooding in some years and surface wetting by precipitation in most years (Bryant, 2003). CPO-driven events also present far shorter durations (average event duration of 81 min) compared to LLJ-driven events (average duration of 234 min). This is predominantly due to the short duration of the high surface winds associated with a CPO (Figure 7, see Table S2 in Supporting Information S1), although there was also some limited evidence that precipitation associated with CPO development could contribute to a reduction in the duration of dust events in some cases.

From Table 1 it should also be noted that over 25% of the total annual horizontal flux of sediment measured at Etosha Pan occurred in “non-events” that did not reach the qualitative threshold value of 0.5 mg/m^3 aerosol concentration used for event identification in this study. There is therefore a meaningful amount of sediment suspended by high frequency and lower velocity winds. Nevertheless, the data in Table 1 confirm the dominance of the lower frequency but higher magnitude events ($>0.5 \text{ mg/m}^3$ aerosol concentration) in generating horizontal dust flux at Etosha Pan.

5. Conclusion

Despite recent remote sensing investigations offering advances in our understanding of the operation of wind-blown dust sources, field measurements of at-source dust emission dynamics remain rare but essential in their contribution. The value of longer-term field experiments is highlighted here with the first year-long data set to quantify windblown dust entrainment mechanisms at a globally significant source of aeolian dust emissions. Using meteorological measurements with co-located aerosol concentration data from five locations around Etosha Pan in Namibia we identified 51 significant dust events over the course of a year, quantifying the horizontal dust flux from this major generative source of mineral aerosols. Our principal findings from the field experiments were:

1. We substantiate the importance to dust emission processes of strong E-ENE winds associated with winter high pressure circulation, with high frequencies of dust events occurring from June to August (Vickery et al., 2013). However, our data also highlight the occurrence of frequent dust events throughout the year with erosion of surface sediment occurring in the austral spring (October and November) and summer (December). Indeed,

- there were no dust-free months in our instrumental record and such persistence in dust events throughout the year has remained unrecognized in the remote sensing record.
2. By quantifying a relative horizontal dust flux associated with dust emission events, we show that dust flux over the annual cycle responds to a complex interplay between erosivity and erodibility variables. In this way, maximum horizontal dust flux is found to occur in November when a desiccated and cracked pan surface at the end of the dry season (Nield et al., 2015; Nield, McKenna Neuman, et al., 2016; Nield, Wiggs, et al., 2016) coincides with strengthening winds, increasing temperatures, and low relative humidity prior to the onset of summer rains. In contrast, the austral autumn (March, April and May) is represented by low horizontal dust fluxes.
 3. Our analysis establishes the marked seasonal differences in the meteorological mechanisms that generate dust uplift between winter and summer. In the winter dry season, dust events are commonly driven by a mixing to the surface of high winds soon after sunrise, associated with the break-down of a low-level jet (LLJ; Clements & Washington, 2021). This mechanism resulted in dust events that were typically sustained until mid-afternoon. LLJ-driven emissions were seen to dominate the annual dust budget, accounting for 61% of events by frequency and 58% of the total annual horizontal dust flux. In contrast, in the more humid summer, dust events were generated by cold pool outflows (CPO) associated with the development of convective systems in the late afternoon and evening. These events were characterized by short periods of intense dust uplift and, whilst they accounted for 39% of events by frequency, they explained only 16% of the total annual horizontal dust flux. The role of LLJ and CPO mechanisms in dust emission from major sources has been previously documented in the Sahara and Sahel (e.g., Allen & Washington, 2014; Bergametti et al., 2022; Provod et al., 2016; Rajot et al., 2008), but we provide the first ground-based data in the southern hemisphere. In quantifying the significance of LLJs and CPOs over a complete annual cycle we have also been able to capture clear seasonal differences in their operation. The occurrence of CPO-driven dust emissions is noteworthy given that the associated meteorological processes that drive CPOs are poorly represented in dust emissions models (Bergametti et al., 2022; Marsham et al., 2013).
 4. We quantify the relative magnitude of dust events and show they are heavily dominated by a few large events, where nearly 31% of all horizontal dust flux is seen to be generated by the six largest events, and a single event accounts for as much as 8%.

Our findings offer confidence in the capacity of remote sensing and dust emissions models to recognize and account for large scale dust emission events that make the principal contribution to the atmospheric aerosol budget. However, with regard to satellite-based approaches for determining dust emission dynamics, our findings highlight the importance of appropriate temporal sampling by sensors to ensure that individual and highly contributing emissions events are not missed due to overpass timing (Baddock et al., 2021; Schepanski et al., 2007). In particular, our ground-based observations linking dust event timing and specific meteorological drivers provide insights for the types of dust events that will be included (and excluded) in satellite-based point source mapping. This understanding sheds more light on the types of dust uplift considered in dust model calibration efforts when the model evaluation is based on inventories of point sources (e.g., Hennen et al., 2022). For example, where convective generated dust events (e.g., CPOs) occur in the evening, MODIS observations will miss these and will not be able to provide a determination of origin point.

Our data also reveal that over 25% of horizontal dust flux across the pan was generated by small erosion episodes which, using the detection threshold used in this study, were not identified as specific emissions events. Our ground-based observations recognize this contribution, and the finding has implications for how such relatively minor (though additively significant) dust activity can be properly accounted for in emissions modeling where it remains “unseen” by remote sensing analysis (Okin et al., 2011; Urban et al., 2018).

Our data clearly demonstrate the value that longer-term (≈ 1 year), ground-based, and at-source field measurements can offer to interpretations of dust event dynamics and characteristics. Critically, they allow a full assessment of the response of emissions processes to seasonally changing drivers of erosivity and erodibility and, significantly, such field data provide an evaluation of the relative magnitude of dust event flux in contrast to event frequency.

Data Availability Statement

The data used in this manuscript can be found in the Oxford University Research Archive: <https://doi.org/10.5287/bodleian:DO706MAYD>, (Wiggs et al., 2022). All EUMETSAT MSG SEVIRI (2022) archive data were provided under Research Project License Number: 50002136 (awarded to R.G. Bryant), via the Eumetsat Data Store (<https://data.eumetsat.int/>)

Acknowledgments

The authors are very grateful to the staff at Etosha National Park for their help and assistance in undertaking the fieldwork, especially Boas Erckie, Pierre du Preez, Claudine Cloete, Immanuel Kapofi, Wilferd Versfeld, and Werner Kilian. The assistance of Gillian Maggs-Kölling at the Gobabeb Namib Research Institute is also gratefully acknowledged, as is the support of Mary Seely and Martin Hipondoka. We are grateful to the Ministry of Environment, Forestry and Tourism in Namibia for permitting the research (permits 1978/2014 and 2140/2016). The research was funded by the Natural Environment Research Council (grant NE/H021841/1) in the UK, and the John Fell Oxford University Press (OUP) Research Fund (121/474).

References

- Allen, C. J. T., & Washington, R. (2014). The low-level jet dust emission mechanism in the central Sahara: Observations from Bordj-Badji Mokhtar during the June 2011 FENNEC intensive observation period. *Journal of Geophysical Research*, 119(6), 2990–3015. <https://doi.org/10.1002/2013jd020594>
- Allen, C. J. T., Washington, R., & Engelstaedter, S. (2013). Dust emission and transport mechanisms in the central Sahara: FENNEC ground-based observations from Bordj Badji Mokhtar, June 2011. *Journal of Geophysical Research: Atmospheres*, 118(12), 6212–6232. <https://doi.org/10.1002/jgrd.50534>
- Allen, C. J. T., Washington, R., & Saci, A. (2015). Dust detection from ground-based observations in the summer global dust maximum: Results from FENNEC 2011 and 2012 and implications for modeling and field observations. *Journal of Geophysical Research*, 120(3), 897–916. <https://doi.org/10.1002/2014jd022655>
- Ashpole, I., & Washington, R. (2013). A new high-resolution central and Western Saharan summertime dust source map from automated satellite dust plume tracking. *Journal of Geophysical Research: Atmospheres*, 118(13), 6981–6995. <https://doi.org/10.1002/jgrd.50554>
- Baddock, M. C., Bryant, R. G., Domínguez Acosta, M., & Gill, T. E. (2021). Understanding dust sources through remote sensing: Making a case for CubeSats. *Journal of Arid Environments*, 184, 104335. <https://doi.org/10.1016/j.jaridenv.2020.104335>
- Baddock, M. C., Ginoux, P., Bullard, J. E., & Gill, T. E. (2016). Do MODIS-defined dust sources have a geomorphological signature? *Geophysical Research Letters*, 43(6), 2606–2613. <https://doi.org/10.1002/2015gl067327>
- Baddock, M. C., Parsons, K., Strong, C., Leys, J., & McTainsh, G. (2015). Drivers of Australian dust: A case study of frontal winds and dust dynamics in the lower Lake Eyre Basin. *Earth Surface Processes and Landforms*, 40(14), 1982–1988. <https://doi.org/10.1002/esp.3773>
- Bergametti, G., Marticorena, B., Rajot, J. L., Foret, G., Alfaro, S. C., & Laurent, B. (2018). Size-resolved dry deposition velocities of dust particles: In situ measurements and parameterizations testing. *Journal of Geophysical Research: Atmospheres*, 123(19), 11080–11099. <https://doi.org/10.1029/2018jd028964>
- Bergametti, G., Rajot, J. L., Marticorena, B., Féron, A., Gaimoz, C., Chatenet, B., et al. (2022). Rain, wind, and dust concentrations in the Sahel. *Journal of Geophysical Research: Atmospheres*, 127(3), e2021JD035802. <https://doi.org/10.1029/2021jd035802>
- Bhattachan, A., D'Odorico, P., & Okin, G. S. (2015). Biogeochemistry of dust sources in Southern Africa. *Journal of Arid Environments*, 117, 18–27. <https://doi.org/10.1016/j.jaridenv.2015.02.013>
- Blackadar, A. K. (1957). Boundary layer wind maxima and their significance for the growth of nocturnal inversions. *Bulletin of the American Meteorological Society*, 38(5), 283–290. <https://doi.org/10.1175/1520-0477-38.5.283>
- Bouet, C., Labiadh, M. T., Rajot, J. L., Bergametti, G., Marticorena, B., des Tureaux, T. H., et al. (2019). Impact of desert dust on air quality: What is the meaningfulness of daily PM standards in regions close to the sources? The example of southern Tunisia. *Atmosphere*, 10(8), 452. <https://doi.org/10.3390/atmos10080452>
- Bristow, C. S., Hudson-Edwards, K. A., & Chappell, A. (2010). Fertilizing the Amazon and equatorial Atlantic with West African dust. *Geophysical Research Letters*, 37(14), L14807. <https://doi.org/10.1029/2010gl043486>
- Bryant, R. G. (2003). Monitoring hydrological controls on dust emissions: Preliminary observations from Etosha Pan, Namibia. *Geographical Journal*, 169(2), 131–141. <https://doi.org/10.1111/1475-4959.04977>
- Bryant, R. G. (2013). Recent advances in our understanding of dust source emission processes. *Progress in Physical Geography*, 37(3), 397–421. <https://doi.org/10.1177/0309133313479391>
- Bryant, R. G., & Baddock, M. C. (2021). Remote sensing of aeolian processes. *Reference Module in Earth Systems and Environmental Sciences*, 84–119. <https://doi.org/10.1016/B978-0-12-818234-5.00132-2>
- Bryant, R. G., Bigg, G. R., Mahowald, N. M., Eckardt, F. D., & Ross, S. G. (2007). Dust emission response to climate in southern Africa. *Journal of Geophysical Research: Atmospheres*, 112(9), D09207. <https://doi.org/10.1029/2005jd007025>
- Buch, M. W., & Rose, D. (1996). Mineralogy and geochemistry of the sediments of the Etosha Pan region in northern Namibia: A reconstruction of the depositional environment. *Journal of African Earth Sciences*, 22(3), 355–378. [https://doi.org/10.1016/0899-5362\(96\)00020-6](https://doi.org/10.1016/0899-5362(96)00020-6)
- Bullard, J. E. (2010). Bridging the gap between field data and global models: Current strategies in aeolian research. *Earth Surface Processes and Landforms*, 35(4), 496–499. <https://doi.org/10.1002/esp.1958>
- Cahill, T. A., Gill, T. E., Reid, J. S., Gearhart, E. A., & Gillette, D. A. (1996). Saltating particles, playa crusts and dust aerosols at Owens (dry) Lake, California. *Earth Surface Processes and Landforms*, 21(7), 621–639. [https://doi.org/10.1002/\(sici\)1096-9837\(199607\)21:7<621::aid-esp661>3.0.co;2-e](https://doi.org/10.1002/(sici)1096-9837(199607)21:7<621::aid-esp661>3.0.co;2-e)
- Cassar, N., Bender, M. L., Barnett, B. A., Fan, S., Moxim, W. J., Levy, H., II, & Tilbrook, B. (2007). The southern ocean biological response to aeolian iron deposition. *Science*, 317(5841), 1067–1070. <https://doi.org/10.1126/science.1144602>
- Caton Harrison, T., Washington, R., & Engelstaedter, S. (2019). A 14-year climatology of Saharan dust emission mechanisms inferred from automatically tracked plumes. *Journal of Geophysical Research: Atmospheres*, 124(16), 9665–9690. <https://doi.org/10.1029/2019jd030291>
- Caton Harrison, T., Washington, R., & Engelstaedter, S. (2021). Satellite-derived characteristics of Saharan cold pool outflows during Boreal summer. *Journal of Geophysical Research: Atmospheres*, 126(3), e2020JD033387. <https://doi.org/10.1029/2020jd033387>
- Clements, M., & Washington, R. (2021). Atmospheric controls on mineral dust emission from the Etosha Pan, Namibia: Observations from the CLARIFY-2016 field campaign. *Journal of Geophysical Research: Atmospheres*, 126(14), e2021JD034746. <https://doi.org/10.1029/2021jd034746>
- Csavina, J., Field, J., Felix, O., Corral-Avitia, A. Y., Saez, A. E., & Betterton, E. A. (2014). Effect of wind speed and relative humidity on atmospheric dust concentrations in semi-arid climates. *Science of the Total Environment*, 487, 82–90. <https://doi.org/10.1016/j.scitotenv.2014.03.138>
- Dansie, A. P., Thomas, D. S. G., Wiggs, G. F. S., Baddock, M. C., & Ashpole, I. (2022). Plumes and Blooms—Locally-sourced Fe-rich aeolian mineral dust drives phytoplankton growth off southwest Africa. *Science of the Total Environment*, 829, 154562. <https://doi.org/10.1016/j.scitotenv.2022.154562>

- Dansie, A. P., Thomas, D. S. G., Wiggs, G. F. S., & Munkittrick, K. R. (2018). Spatial variability of ocean fertilizing nutrients in the dust-emitting ephemeral river catchments of Namibia. *Earth Surface Processes and Landforms*, 43(3), 563–578. <https://doi.org/10.1002/esp.4207>
- Dansie, A. P., Wiggs, G. F. S., Thomas, D. S. G., & Washington, R. (2017). Measurements of windblown dust characteristics and ocean fertilization potential: The ephemeral river valleys of Namibia. *Aeolian Research*, 29, 30–41. <https://doi.org/10.1016/j.aeolia.2017.08.002>
- Darmenova, K., Sokolik, I. N., Shao, Y., Marticorena, B., & Bergametti, G. (2009). Development of a physically-based dust emission module within the Weather Research and Forecasting (WRF) model: Assessment of dust emission parameterizations and input parameters for source regions in Central and East Asia. *Journal of Geophysical Research*, 114(D14), D14201. <https://doi.org/10.1029/2008JD011236>
- Draxler, R. R., Gillette, D. A., Kirkpatrick, J. S., & Heller, J. (2001). Estimating PM10 air concentrations from dust storms in Iraq, Kuwait and Saudi Arabia. *Atmospheric Environment*, 35(25), 4315–4330. [https://doi.org/10.1016/s1352-2310\(01\)00159-5](https://doi.org/10.1016/s1352-2310(01)00159-5)
- Emmel, C., Knippertz, P., & Schulz, O. (2010). Climatology of convective density currents in the southern foothills of the Atlas Mountains. *Journal of Geophysical Research*, 115(D11), D11115. <https://doi.org/10.1029/2009jd012863>
- Engert, S. (1997). Spatial variability and temporal periodicity of rainfall in the Etosha National Park and surrounding areas in northern Namibia. *Madoqua*, 1, 115–120.
- EUMETSAT (MSG SEVIRI). (2022). [Dataset]. <https://data.eumetsat.int/>
- Evan, A. T., Flamant, C., Gaetani, M., & Guichard, F. (2016). The past, present and future of African dust. *Nature*, 531(7595), 493–495. <https://doi.org/10.1038/nature17149>
- Fiedler, S., Schepanski, K., Heinold, B., Knippertz, P., & Tegen, I. (2013). Climatology of nocturnal low-level jets over North Africa and implications for modeling mineral dust emission. *Journal of Geophysical Research: Atmospheres*, 118(12), 6100–6121. <https://doi.org/10.1002/jgrd.50394>
- Ge, J. M., Liu, H., Huang, J., & Fu, Q. (2016). Taklimakan desert nocturnal low-level jet: Climatology and dust activity. *Atmospheric Chemistry and Physics*, 16(12), 7773–7783. <https://doi.org/10.5194/acp-16-7773-2016>
- Gillette, D. A., Fryrear, D. W., Gill, T. E., Ley, T., Cahill, T. A., & Gerhart, E. A. (1997). Relation of vertical flux of particles smaller than 10 μ m to total aeolian horizontal mass flux at Owens Lake. *Journal of Geophysical Research*, 102(D22), 26009–26015. <https://doi.org/10.1029/97jd02252>
- Ginoux, P., Prospero, J. M., Gill, T. E., Hsu, N. C., & Zhao, M. (2012). Global-scale attribution of anthropogenic and natural dust sources and their emission rates based on MODIS Deep Blue aerosol products. *Reviews of Geophysics*, 50(3), RG3005. <https://doi.org/10.1029/2012RG000388>
- Goldstein, H. L., Breit, G. N., & Reynolds, R. L. (2017). Controls on the chemical composition of saline surface crusts and emitted dust from a wet playa in the Mojave Desert (USA). *Journal of Arid Environments*, 140, 50–66. <https://doi.org/10.1016/j.jaridenv.2017.01.010>
- Gong, S. L., & Zhang, X. Y. (2008). CUACE/Dust—An integrated system of observation and modeling systems for operational dust forecasting in Asia. *Atmospheric Chemistry and Physics*, 8(9), 2333–2340. <https://doi.org/10.5194/acp-8-2333-2008>
- Hausein, K., Washington, R., King, J., Wiggs, G., Thomas, D. S. G., Eckardt, F. D., et al. (2015). Testing the performance of state-of-the-art dust emission schemes using DO4Models field data. *Geoscientific Model Development*, 8(2), 341–362. <https://doi.org/10.5194/gmd-8-341-2015>
- Hennen, M., Chappell, A., Edwards, B. L., Faist, A. M., Kandakji, T., Baddock, M. C., et al. (2022). A North American dust emission climatology (2001–2020) calibrated to dust point sources from satellite observations. *Aeolian Research*, 54, 100766. <https://doi.org/10.1016/j.aeolia.2021.100766>
- Hipondoka, M. H. T., Mauz, B., Kempf, J., Packman, S., Chiverrell, R. C., & Bloemendal, J. (2014). Chronology of sand ridges and the late quaternary evolution of the Etosha Pan, Namibia. *Geomorphology*, 204, 553–563. <https://doi.org/10.1016/j.geomorph.2013.08.034>
- Ito, A., & Kok, J. F. (2017). Do dust emissions from sparsely vegetated regions dominate atmospheric iron supply to the Southern Ocean? *Journal of Geophysical Research*, 122(7), 3987–4002. <https://doi.org/10.1002/2016jd025939>
- Jickells, T. D., An, Z. S., Andersen, K. K., Baker, A. R., Bergametti, G., Brooks, N., et al. (2005). Global iron connections between desert dust, ocean biogeochemistry, and climate. *Science*, 308(5718), 67–71. <https://doi.org/10.1126/science.1105959>
- Kaly, F., Marticorena, B., Chatenet, B., Rajot, J. L., Janicot, S., Niang, A., et al. (2015). Variability of mineral dust concentrations over West Africa monitored by the Sahelian dust transect. *Atmospheric Research*, 164–165, 226–241. <https://doi.org/10.1016/j.atmosres.2015.05.011>
- Khalfallah, B., Bouet, C., Labiadh, M. T., Alfaro, S. C., Bergametti, G., Marticorena, B., et al. (2020). Influence of atmospheric stability on the size distribution of the vertical dust flux measured in eroding conditions over a flat bare sandy field. *Journal of Geophysical Research: Atmospheres*, 125(4), e2019JD031185. <https://doi.org/10.1029/2019jd031185>
- Klose, M., Gill, T. E., Etyezian, V., Nikolich, G., Zadeh, Z. G., Webb, N. P., & Van Pelt, R. S. (2019). Dust emission from crusted surfaces: Insights from field measurements and modelling. *Aeolian Research*, 40, 1–14. <https://doi.org/10.1016/j.aeolia.2019.05.001>
- Knippertz, P., Deutscher, C., Kandler, K., Müller, T., Schulz, O., & Schütz, L. (2007). Dust mobilization due to density currents in the Atlas region: Observations from the Saharan Mineral Dust Experiment 2006 field campaign. *Journal of Geophysical Research: Atmospheres*, 112(21), D21109. <https://doi.org/10.1029/2007jd008774>
- Kok, J. F., Albani, S., Mahowald, N. M., & Ward, D. S. (2014b). An improved dust emission model—Part 2: Evaluation in the community earth system model, with implications for the use of dust source functions. *Atmospheric Chemistry and Physics*, 14(23), 13043–13061. <https://doi.org/10.5194/acp-14-13043-2014>
- Kok, J. F., Mahowald, N. M., Fratini, G., Gillies, J. A., Ishizuka, M., Leys, J. F., et al. (2014). An improved dust emission model—Part 1: Model description and comparison against measurements. *Atmospheric Chemistry and Physics*, 14(23), 13023–13041. <https://doi.org/10.5194/acp-14-13023-2014>
- Kok, J. F., Ridley, D. A., Zhou, Q., Miller, R. L., Zhao, C., Heald, C. L., et al. (2017). Smaller desert dust cooling effect estimated from analysis of dust size and abundance. *Nature Geoscience*, 10(4), 274–278. <https://doi.org/10.1038/ngeo2912>
- Koren, I., Kaufman, Y. J., Washington, R., Todd, M. C., Rudich, Y., Vanderlei Martins, J., & Rosenfeld, D. (2006). The Bodélé depression: A single spot in the Sahara that provides most of the mineral dust to the Amazon forest. *Environmental Research Letters*, 1(1), 014005. <https://doi.org/10.1088/1748-9326/1/1/014005>
- Lawrence, C. R., Reynolds, R. L., Ketterer, M. E., & Neff, J. C. (2013). Aeolian controls of soil geochemistry and weathering fluxes in high-elevation ecosystems of the Rocky Mountains, Colorado. *Geochimica et Cosmochimica Acta*, 107, 27–46. <https://doi.org/10.1016/j.gca.2012.12.023>
- Lee, J. A., Gill, T. E., Mulligan, K. R., Acosta, M. D., & Perez, A. E. (2009). Land use/landcover and point sources of the 15 December 2003 dust storm in southwestern North America. *Geomorphology*, 105(1–2), 18–27. <https://doi.org/10.1016/j.geomorph.2007.12.016>
- Leys, J. F., Heidenreich, S. K., Strong, C. L., McTainsh, G. H., & Quigley, S. (2011). PM10 concentrations and mass transport during “Red Dawn”—Sydney 23 September 2009. *Aeolian Research*, 3(3), 327–342. <https://doi.org/10.1016/j.aeolia.2011.06.003>
- Li, F., Vogelmann, A. M., & Ramanathan, V. (2004). Saharan dust aerosol radiative forcing measured from space. *Journal of Climate*, 17(13), 2558–2571. [https://doi.org/10.1175/1520-0442\(2004\)017<2558:sdarfms>2.0.co;2](https://doi.org/10.1175/1520-0442(2004)017<2558:sdarfms>2.0.co;2)

- Mahowald, N. M., Bryant, R. G., del Corral, J., & Steinberger, L. (2003). Ephemeral lakes and desert dust sources. *Geophysical Research Letters*, 30(2), 461–464. <https://doi.org/10.1029/2002gl016041>
- Marshall, J. H., Hobby, M., Allen, C. J. T., Banks, J. R., Bart, M., Brooks, B. J., et al. (2013). Meteorology and dust in the central Sahara: Observations from FENNEC supersite-1 during the June 2011 intensive observation period. *Journal of Geophysical Research: Atmospheres*, 118(10), 4069–4089. <https://doi.org/10.1002/jgrd.50211>
- Marshall, J. H., Knippertz, P., Dixon, N. S., Parker, D. J., & Lister, G. M. S. (2011). The importance of the representation of deep convection for modeled dust-generating winds over West Africa during summer. *Geophysical Research Letters*, 38(16), L16803. <https://doi.org/10.1029/2011gl048368>
- Marshall, J. H., Parker, D. J., Grams, C. M., Taylor, C. M., & Haywood, J. M. (2008). Uplift of Saharan dust south of the intertropical discontinuity. *Journal of Geophysical Research: Atmospheres*, 113(21), D21102. <https://doi.org/10.1029/2008jd009844>
- Marticorena, B., Chatenet, B., Rajot, J. L., Bergametti, G., Deroubaix, A., Vincent, J., et al. (2017). Mineral dust over west and central Sahel: Seasonal patterns of dry and wet deposition fluxes from a pluriannual sampling (2006–2012). *Journal of Geophysical Research*, 122(2), 1338–1364. <https://doi.org/10.1002/2016jd025995>
- Marticorena, B., Chatenet, B., Rajot, J. L., Traoré, S., Coulibaly, M., Diallo, A., et al. (2010). Temporal variability of mineral dust concentrations over West Africa: Analyses of a pluriannual monitoring from the AMMA Sahelian Dust Transect. *Atmospheric Chemistry and Physics*, 10(18), 8899–8915. <https://doi.org/10.5194/acp-10-8899-2010>
- McTainsh, G., Chan, Y.-C., McGowan, H., Leys, J., & Tews, K. (2005). The 23rd October 2002 dust storm in eastern Australia: Characteristics and meteorological conditions. *Atmospheric Environment*, 39(7), 1227–1236. <https://doi.org/10.1016/j.atmosenv.2004.10.016>
- Mendelsohn, J., Jarvis, A., & Robertson, T. (Eds.) (2013). *A profile and Atlas of the Cuvelai-Etoshia Basin*. Raison & Gondwana Collection. 166.
- Miller, S. D., Kuciauskas, A. P., Liu, M., Ji, Q., Reid, J. S., Breed, D. W., et al. (2008). Haboob dust storms of the southern Arabian Peninsula. *Journal of Geophysical Research: Atmospheres*, 113(1), D01202. <https://doi.org/10.1029/2007jd008550>
- Mockford, T., Bullard, J. E., & Thorsteinsson, T. (2018). The dynamic effects of sediment availability on the relationship between wind speed and dust concentration. *Earth Surface Processes and Landforms*, 43(11), 2484–2492. <https://doi.org/10.1002/esp.4407>
- Murray, J. E., Brindley, H. E., Bryant, R. G., Russell, J. E., Jenkins, K. F., & Washington, R. (2016). Enhancing weak transient signals in SEVIRI false color imagery: Application to dust source detection in southern Africa. *Journal of Geophysical Research*, 121(17), 10199–10219. <https://doi.org/10.1002/2016jd025221>
- Nield, J. M., Bryant, R. G., Wiggs, G. F. S., King, J., Thomas, D. S. G., Eckardt, F. D., & Washington, R. (2015). The dynamism of salt crust patterns on playas. *Geology*, 43(1), 31–34. <https://doi.org/10.1130/g36175.1>
- Nield, J. M., McKenna Neuman, C., O'Brien, P., Bryant, R. G., & Wiggs, G. F. S. (2016). Evaporative sodium salt crust development and its wind tunnel derived transport dynamics under variable climatic conditions. *Aeolian Research*, 23, 51–62. <https://doi.org/10.1016/j.aeolia.2016.09.003>
- Nield, J. M., Wiggs, G. F. S., King, J., Bryant, R. G., Eckardt, F. D., Thomas, D. S. G., & Washington, R. (2016). Climate-surface-pore-water interactions on a salt crusted playa: Implications for crust pattern and surface roughness development measured using terrestrial laser scanning. *Earth Surface Processes and Landforms*, 41(6), 738–753. <https://doi.org/10.1002/esp.3860>
- Niemeyer, T. C., Gillette, D. A., Deluisi, J. J., Kim, Y. J., Niemeyer, W. F., Ley, T., et al. (1999). Optical depth, size distribution and flux of dust from Owens Lake, California. *Earth Surface Processes and Landforms*, 24(5), 463–479. [https://doi.org/10.1002/\(sici\)1096-9837\(199905\)24:5<463::aid-esp2>3.0.co;2-r](https://doi.org/10.1002/(sici)1096-9837(199905)24:5<463::aid-esp2>3.0.co;2-r)
- O'Hara, S. L., Wiggs, G. F. S., Mamedov, B., Davidson, G., & Hubbard, R. B. (2000). Exposure to airborne dust contaminated with pesticide in the Aral Sea region. *Lancet*, 355(9204), 627–628. [https://doi.org/10.1016/s0140-6736\(99\)04753-4](https://doi.org/10.1016/s0140-6736(99)04753-4)
- Okin, G. S., Bullard, J. E., Reynolds, R. L., Ballantine, J. A. C., Schepanski, K., Todd, M. C., et al. (2011). Dust: Small-scale processes with global consequences. *Eos, Transactions American Geophysical Union*, 92(29), 241–242. <https://doi.org/10.1029/2011eo290001>
- Parker, D. J., Burton, R. R., Diongue-Niang, A., Ellis, R. J., Felton, M., Taylor, C. M., et al. (2005). The diurnal cycle of the West African monsoon circulation. *Quarterly Journal of the Royal Meteorological Society*, 131(611), 2839–2860. <https://doi.org/10.1256/qj.04.52>
- Preston-Whyte, R. A., Diab, R. D., & Sokolic, F. (1994). Thermo—Topographically induced winds in the boundary layer over the Etosha Pan. *South African Geographical Journal*, 76(2), 59–62. <https://doi.org/10.1080/03736245.1994.9713576>
- Prospero, J. M., Collard, F.-X., Molinié, J., & Jeannot, A. (2014). Characterizing the annual cycle of African dust transport to the Caribbean Basin and South America and its impact on the environment and air quality. *Global Biogeochemical Cycles*, 28(7), 757–773. <https://doi.org/10.1002/2013gb004802>
- Prospero, J. M., Ginoux, P., Torres, O., Nicholson, S. E., & Gill, T. E. (2002). Environmental characterization of global sources of atmospheric soil dust identified with the Nimbus 7 Total Ozone Mapping Spectrometer (TOMS) absorbing aerosol product. *Reviews of Geophysics*, 40(1), 1002. <https://doi.org/10.1029/2000RG000095>
- Provod, M., Marshall, J. H., Parker, D. J., & Birch, C. E. (2016). A characterisation of cold pools in the West African Sahel. *Monthly Weather Review*, 144(5), 1923–1934. <https://doi.org/10.1175/mwr-d-15-0023.1>
- Rajot, J. L., Formenti, P., Alfaro, S., Desboeufs, K., Chevaillier, S., Chatenet, B., et al. (2008). AMMA dust experiment: An overview of measurements performed during the dry season special observation period (SOP0) at the Banizoumbou (Niger) supersite. *Journal of Geophysical Research: Atmospheres*, 113(23), D00C14. <https://doi.org/10.1029/2008jd009906>
- Reid, J. S., Flocchini, R. G., Cahill, T. A., Ruth, R. S., & Salgado, D. P. (1994). Local meteorological, transport, and source aerosol characteristics of late autumn Owens Lake (dry) dust storms. *Atmospheric Environment*, 28(9), 1699–1706. [https://doi.org/10.1016/1352-2310\(94\)90315-8](https://doi.org/10.1016/1352-2310(94)90315-8)
- Schepanski, K. (2018). Transport of mineral dust and its impact on climate. *Geosciences*, 8(5), 151. <https://doi.org/10.3390/geosciences8050151>
- Schepanski, K., Tegen, I., Laurent, B., Heinold, B., & Macke, A. (2007). A new Saharan dust source activation frequency map derived from MSG-SEVIRI IR-channels. *Geophysical Research Letters*, 34(18), L18803. <https://doi.org/10.1029/2007GL030168>
- Schepanski, K., Tegen, I., Todd, M. C., Heinold, B., Bönisch, G., Laurent, B., & Macke, A. (2009). Meteorological processes forcing Saharan dust emission inferred from MSG-SEVIRI observations of subdaily dust source activation and numerical models. *Journal of Geophysical Research: Atmospheres*, 114(10), D10201. <https://doi.org/10.1029/2008jd010325>
- Shao, Y., Wyrwoll, K. H., Chappell, A., Huang, J., Lin, Z., McTainsh, G. H., et al. (2011). Dust cycle: An emerging core theme in Earth system science. *Aeolian Research*, 2(4), 181–204. <https://doi.org/10.1016/j.aeolia.2011.02.001>
- Shao, Y., Zhang, J., Ishizuka, M., Mikami, M., Leys, J., & Huang, N. (2020). Dependency of particle size distribution at dust emission on friction velocity and atmospheric boundary-layer stability. *Atmospheric Chemistry and Physics*, 20(21), 12939–12953. <https://doi.org/10.5194/acp-20-12939-2020>
- Slingo, A., Ackerman, T. P., Allan, R. P., Kassianov, E. I., McFarlane, S. A., Robinson, G. J., et al. (2006). Observations of the impact of a major Saharan dust storm on the atmospheric radiation balance. *Geophysical Research Letters*, 33(24), L24817. <https://doi.org/10.1029/2006gl027869>

- Sokolik, I. N., & Toon, O. B. (1999). Incorporation of mineralogical composition into models of the radiative properties of mineral aerosol from UV to IR wavelengths. *Journal of Geophysical Research: Atmospheres*, *104*(D8), 9423–9444. <https://doi.org/10.1029/1998jd200048>
- Sow, M., Alfaro, S. C., Rajot, J. L., & Marticorena, B. (2009). Size resolved dust emission fluxes measured in Niger during 3 dust storms of the AMMA experiment. *Atmospheric Chemistry and Physics*, *9*(12), 3881–3891. <https://doi.org/10.5194/acp-9-3881-2009>
- Stafoggia, M., Zauli-Sajani, S., Pey, J., Samoli, E., Alessandrini, E., Basagaña, X., et al. (2016). Desert dust outbreaks in Southern Europe: Contribution to daily PM10 concentrations and short-term associations with mortality and hospital admissions. *Environmental Health Perspectives*, *124*(4), 413–419. <https://doi.org/10.1289/ehp.1409164>
- Todd, M. C., Allen, C. J. T., Bart, M., Bechir, M., Bentefouet, J., Brooks, B. J., et al. (2013). Meteorological and dust aerosol conditions over the Western Saharan region observed at FENNEC Supersite-2 during the intensive observation period in June 2011. *Journal of Geophysical Research: Atmospheres*, *118*(15), 8426–8447. <https://doi.org/10.1002/jgrd.50470>
- Todd, M. C., Washington, R., Vanderlei Martins, J., Dubovik, O., Lizcano, G., M'Bainayel, S., & Engelstaedter, S. (2007). Mineral dust emission from the Bodélé depression northern Chad, during BoDEX 2005. *Journal of Geophysical Research: Atmospheres*, *112*(6), D06207. <https://doi.org/10.1029/2006jd007170>
- Tyson, P. D., & Preston-Whyte, R. A. (2015). *The weather and climate of southern Africa* (2nd edn). Oxford University Press. 395.
- Urban, F. E., Goldstein, H. L., Fulton, R., & Reynolds, R. L. (2018). Unseen dust emission and global dust abundance: Documenting dust emission from the Mojave desert (USA) by daily remote camera imagery and wind-erosion measurements. *Journal of Geophysical Research: Atmospheres*, *123*(16), 8735–8753. <https://doi.org/10.1029/2018jd028466>
- Vickery, K. J., Eckardt, F. D., & Bryant, R. G. (2013). A sub-basin scale dust plume source frequency inventory for southern Africa, 2005–2008. *Geophysical Research Letters*, *40*(19), 5274–5279. <https://doi.org/10.1002/grl.50968>
- von Holdt, J. R., Eckardt, F. D., & Wiggs, G. F. S. (2017). Landsat identifies aeolian dust emission dynamics at the landform scale. *Remote Sensing of Environment*, *198*, 229–243. <https://doi.org/10.1016/j.rse.2017.06.010>
- von Holdt, J. R. C., Eckardt, F. D., Baddock, M. C., & Wiggs, G. F. S. (2019). Assessing landscape dust emission potential using combined ground-based measurements and remote sensing data. *Journal of Geophysical Research, Earth Surface*, *124*(5), 1080–1098. <https://doi.org/10.1029/2018jf004713>
- Wang, X., Chancellor, G., Evenstad, J., Farnsworth, J. E., Hase, A., Olson, G. M., et al. (2009). A novel optical instrument for estimating size segregated aerosol mass concentration in real time. *Aerosol Science and Technology*, *43*(9), 939–950. <https://doi.org/10.1080/02786820903045141>
- Wang, Y. Q., Zhang, X. Y., Gong, S. L., Zhou, C. H., Hu, X. Q., Liu, H. L., et al. (2008). Surface observation of sand and dust storm in East Asia and its application in CUACE/Dust. *Atmospheric Chemistry and Physics*, *8*(3), 545–553. <https://doi.org/10.5194/acp-8-545-2008>
- Washington, R., Todd, M., Middleton, N. J., & Goudie, A. S. (2003). Dust-storm source areas determined by the total ozone monitoring spectrometer and surface observations. *Annals of the Association of American Geographers*, *93*(2), 297–313. <https://doi.org/10.1111/1467-8306.9302003>
- Washington, R., & Todd, M. C. (2005). Atmospheric controls on mineral dust emission from the Bodélé depression, Chad: The role of the low level jet. *Geophysical Research Letters*, *32*(17), L17701–L17705. <https://doi.org/10.1029/2005gl023597>
- Washington, R., Todd, M. C., Engelstaedter, S., M' Bainayel, S., & Mitchell, F. (2006). Dust and the low-level circulation over the Bodélé depression, Chad: Observations from BoDEX 2005. *Journal of Geophysical Research: Atmospheres*, *111*(3), D03201. <https://doi.org/10.1029/2005jd006502>
- Watson, J. G., Chow, J. C., Chen, L., Wang, X., Merrifield, T. M., Fine, P. M., & Barker, K. (2011). Measurement system evaluation for upwind/downwind sampling of fugitive dust emissions. *Aerosol and Air Quality Research*, *11*(4), 331–350. <https://doi.org/10.4209/aaqr.2011.03.0028>
- Webb, N. P., LeGrand, S. L., Cooper, B. F., Courtright, E. M., Edwards, B. L., Felt, C., et al. (2021). Size distribution of mineral dust emissions from sparsely vegetated and supply-limited dryland soils. *Journal of Geophysical Research: Atmospheres*, *126*(22), e2021JD035478. <https://doi.org/10.1029/2021jd035478>
- Wiggs, G. F. S., Baddock, M. C., Thomas, D. S. G., Washington, R., Nield, J. N., Engelstaedter, S., et al. (2022). Aerosol concentration and meteorological data at Etosha Pan, Namibia [Dataset]. STL, Retrieved from <https://ora.ox.ac.uk/objects/uuid:95135c39-0be4-4fea-9245-287ba63d1a5c>
- Zhang, X. X., Sharratt, B., Liu, L. Y., Wang, Z. F., Pan, X. L., Lei, J. Q., et al. (2018). East Asian dust storm in May 2017: Observations, modelling, and its influence on the Asia-Pacific region. *Atmospheric Chemistry and Physics*, *18*(11), 8353–8371. <https://doi.org/10.5194/acp-18-8353-2018>
- Zhao, A., Ryder, C. L., & Wilcox, L. J. (2022). How well do the CMIP6 models simulate dust aerosols? *Atmospheric Chemistry and Physics*, *22*(3), 2095–2119. <https://doi.org/10.5194/acp-22-2095-2022>
- Zhu, A., Ramanathan, V., Li, F., & Kim, D. (2007). Dust plumes over the Pacific, Indian, and Atlantic Oceans: Climatology and radiative impact. *Journal of Geophysical Research*, *112*(16), D16208. <https://doi.org/10.1029/2007jd008427>
- Zobeck, T. M., & Van Pelt, R. S. (2006). Wind-induced dust generation and transport mechanics on a bare agricultural field. *Journal of Hazardous Materials*, *132*(1), 26–38. <https://doi.org/10.1016/j.jhazmat.2005.11.090>
- Zunckel, M., Held, G., Preston-Whyte, R. A., & Joubert, A. (1996). Low-level wind maxima and the transport of pyrogenic products over southern Africa. *Journal of Geophysical Research: Atmospheres*, *101*(19), 23745–23755. <https://doi.org/10.1029/95jd02602>
- Zunckel, M., Hong, Y., Brassel, K., & O'Beirne, S. (1996). Characteristics of the nocturnal boundary layer: Okaukuejo, Namibia, during SAFARI-92. *Journal of Geophysical Research: Atmospheres*, *101*(19), 23757–23766. <https://doi.org/10.1029/95jd00624>

References From the Supporting Information

- Lensky, I. M., & Rosenfeld, D. (2008). Clouds-Aerosols-Precipitation Satellite Analysis Tool (CAPSAT). *Atmospheric Chemistry and Physics*, *8*, 6739–6753.